Supplementary Information

Brain Charts for the Rhesus Macaque Lifespan

Alldritt, S.S.[1], Ramirez, J.S.B.[2,3], Vos de Wael R.[2], Bethlehem R.[4], Seidlitz J.[5], Nenning K.[6], Smallwood J.[7], Wang Z.[2], Esper, N.B.[2], Franco, A.R.[2,6], Alexander-Bloch A.[8,9], Amaral, D.G.[10,11], Amiez C.[12], Balezeau F.[13], Baxter, M.G.[14], Becker G.[15], Bennett J.[16], Berkner O.[17], Blezer, E.L.A.[18], Brambrink, A.M.[19], Brochier T.[20], Butler B.[21], Byeon K.[2], Campos, L.J.[11], Canet-Soulas E.[15], Chalet L.[22], Chen A.[23], Cléry J.[24], Constantinidis C.[25], Cook, D.J.[7], Dehaene S.[26], Dorfschmidt L.[5], Drzewiecki, C.M.[11], Erdman, J.W.[27], Everling S.[28], Falchier A.[21], Fleysher L.[29], Fox A.[11], Freiwald W.[30], Froesel M.[31], Froudist-Walsh S.[32], Fudge J.[33], Funck T.[2], Gacoin M.[31], Gale, D.J.[34], Gallivan J.[7], Garin, C.M.[35,25], Griffiths, T.D.[13], Guedj C.[36], Hadj-Bouziane F.[37], Hamed, S.B.[31], Harel N.[3], Hartig R.[17], Heuer K.[38], Hiba B.[31], Howell, B.R.[39,40,41], Jarraya B.[26], Jung B.[5], Kalin N.[42], Karpf J.[43], Kastner S.[44], Klink C.[45], Kovacs-Balint, Z.A.[46], Kroenke C.[43], Kuchan, M.J.[47], Kwok, S.C.[48], Lala, K.N.[49], Leopold, D.A.[50], Li G.[51], Lindenfors P.[52,53], Linn G.[17], Mars, R.B.[54], Masiello K.[17], Menon, R.S.[55], Messinger A.[50], Meunier M.[37], Mok K.[24], Morrison, J.H.[56], Nacef J.[13], Nagy J.[57], Neudecker V.[19], Neuringer M.[58], Noonan, M.P.[59], Ortiz-Rios M.[60], Perez-Zoghbi, J.F.[19], Pinsk M.[61], Poirier C.[13], Procyk E.[12], Rajimehr R.[62], Reader, S.M.[63,64], Rudko, D.A.[24], Rushworth, M.F.S.[54], Russ, B.E.[17], Sallet J.[65,54], Sanchez, M.M.[66,46], Schmid, M.C.[67], Schwiedrzik, C.M.[68,69,70], Scott, J.A.[71], Sein J.[20], Sharma, K.K.[33], Shmuel A.[24], Styner M.[51], Sullivan, E.L.[58], Thiele A.[13], Todorov, O.S.[72], Toro R.[38], Tsao D.[73], Tusche A.[7], Vlasova R.[51], Wang L.[23], Wang Z.[74], Wang J.[75], Weiss, A.R.[43], Wilson, C.R.E.[76], Yacoub E.[3], Zarco W.[77], Zhou Y.[78], Zhu J.[25], Petkov, C.I.[79], Margulies D.[80], Fair D.[3], Schroeder C.[81,82], Milham M.[2,6], Xu T.[1*]

Corresponding authors:
Ting Xu: ting.xu@childmind.org

Supplementary Information

1. Data Information

1.1. Data Demographics

In this study, we aggregated data from 1,228 macaques, including 1,861 scans from 33 research studies. The total volume of cortical gray matter, white matter, subcortical gray matter, and ventricles for prenatal macaques (N=28) were extracted from a previously published study[1]. Postnatal MRI data, comprising 1,776 scans from 1,198 macaques, were aggregated and preprocessed using a standardized pipeline. After quality control (see section **S2.2**), 1,024 macaques and 1,522 scans were included in the developmental modeling in GAMLSS. **Fig. S1.1-1** illustrates the age distribution of the macaque data included in the final analyses. **Table S1.1-2** details the number of scans and macaques per research site before and after quality control.

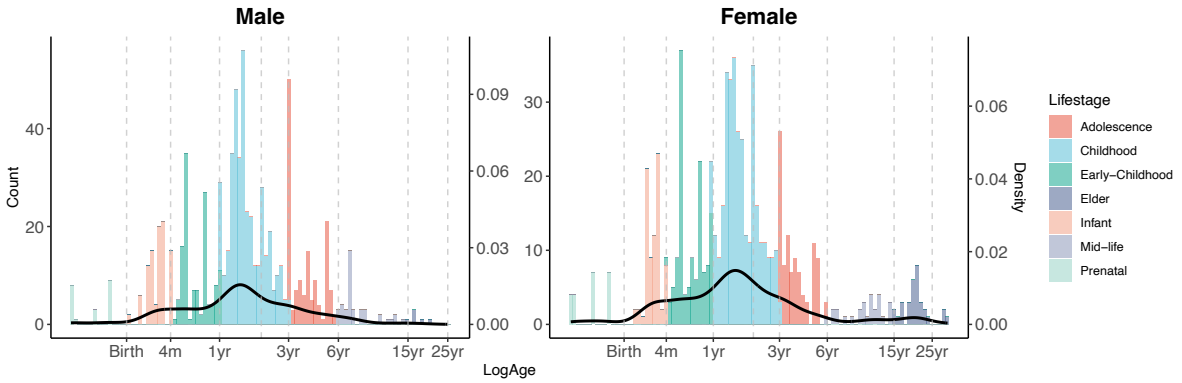

Fig. S1.1-1 | Histogram distribution of ages, stratified by sex. The colored bars represent approximate life stages of macaque. The histograms are displayed on a log scale of age.

Table S1.1-2 | Total demographic distributions by site.

Study site	Animals	M/F	Scans	Age (min - max)	Animals (Post QC)	Scans (Post QC)
site-amu	4	3/1	4	7.5 (7 - 8)	4	4
site-amu-2	20	14/6	21	7.28 (3.13 - 17.64)	15	15
site-ecnu	4	4/0	4	3.4 (2.67 - 3.75)	4	4
site-ecnu-chen	10	10/0	10	N.A	0	0
site-emory	148	82/66	148	0.58 (0.04 - 1.5)	40	83
site-ion	8	7/1	8	5.02 (3.8 - 5.81)	8	8
site-kmust	31	8/23	31	14.23 (10 - 20)	30	30
site-lyon	4	0/4	4	N.A	0	0
site-mcgill	1	0/1	1	12 (12 - 12)	0	0

site-mountsinai-P	8	8/0	8	4.4 (3.4 - 5.1)	8	8
site-mountsinai-S	5	5/0	5	5.94 (5.3 - 6.3)	5	5
site-neurodev	33	18/15	160	1.06 (0 - 3)	33	148
site-newcastle	14	12/2	14	7.53 (3.9 - 13.14)	0	0
site-NIMH	3	1/2	3	6 (5 - 7)	0	0
site-NIMH-CT	3	2/1	3	4.67 (3 - 6)	0	0
site-nin	2	2/0	2	4.5 (4-5)	0	0
site-nki	2	1/1	2	6.5 (6 - 7)	2	2
site-NKIdev	3	1/2	84	0.62 (0.06 - 1.52)	3	83
site-ohsu	2	2/0	2	5 (5 - 5)	0	0
site-OHSU-CU	24	12/12	24	2.09 (1 - 2.93)	23	23
site-OHSU-fetal	28	13/15	84	-0.16 (-0.23 - -0.08)	28	43
site-OHSU-UIUC	22	10/12	65	0.33 (0.16 - 0.5)	22	56
site-oxford	20	20/0	20	4.01 (2.41 - 6.72)	19	19
site-princeton	2	2/0	2	3 (3 - 3)	0	0
site-queens	13	13/0	13	7.31 (6 - 12)	13	13
site-rockefeller	6	6/0	6	N.A	0	0
site-sbri	16	9/7	16	7.02 (3.6 - 13.7)	15	15
site-ucdavis	19	0/19	19	20.38 (18.6 - 22.5)	19	19
site-ucdavis-2	56	28/28	385	1.13 (0.02 - 11.48)	54	265
site-ucdavis-3	94	50/44	94	2.94 (2 - 6)	90	90
site-uminn	2	0/2	2	N.A	0	0
site-uwmadison	584	322/262	584	1.91 (0.84 - 4.42)	572	572
site-uwo	12	12/0	12	5.33 (4 - 8)	2	2
site-wake-forest	21	0/21	21	10.81 (2.53 - 30.64)	15	15
Total	**1224**	**677/547**	**1861**	**2.27 (-0.23 - 30.64)**	**1024**	**1522**

2. Data Preprocessing, Quality Control, and Harmonization

The raw T1-weighted (and T2-weighted, if available) MRI scans of for postnatal data obtained from 23 sites were preprocessed on the high-performance computing system through the Advanced Cyberinfrastructure Coordination Ecosystem: Services and Support (ACCESS: https://access-ci.org). The preprocessing steps included denoising, brain extraction, tissue segmentation, and surface reconstruction (**S2.1.1-S2.1.2**). To ensure the quality of the preprocessing, visual inspections were performed after each step (**S2.2.1-1**). **Supplementary Table 1.2-2** provides details on the number of animals and scans per site before and after preprocessing and quality control. The pipeline was effective for most scans with an age over

4 months. For data that did not pass through the pipeline (a subset of failed infant scans with age < 4 months), we customized the atlases used in the segmentation step and performed manual edits to correct the brain segmentation, facilitating accurate surface reconstruction (**S2.1.2**). Quality control procedures were conducted to ensure the accuracy of the preprocessed data. In total, 1,522 out of 1,861 scans successfully passed the preprocessing and quality controls were used in the lifespan model. To minimize variance in the preprocessing, we conducted data harmonization (**S2.3**) and pipeline validation (**S2.3.2**). Total tissue volumes were extracted from the aseg.stats output from the FreeSurfer 'recon-all' process. Similar to the human study[2], we extracted 'Total gray matter volume' which includes cortical, subcortical, and cerebellum gray matter as GMV; 'Total cortical/cerebral (FreeSurfer version 7.3.2) white matter volume' for WMV; 'Subcortical gray matter volume' for sGMV (inclusive of thalamus, caudate nucleus, putamen, pallidum, hippocampus, amygdala, and nucleus accumbens area); and 'Lateral Ventricles' for ventricular volume. The regional volume, cortical thickness, and surface area were estimated for each 91 bilaterally-averaged cortical regions using the Markov parcellation (**Fig. S4-1**)[3].

2.1 Data Preprocessing

2.1.1 Denoising and Brain Extraction

The raw T1w and T1w images were first denoised using the adaptive non-local means denoising algorithm via the ANTs DenoiseImage function to eliminate salt-and-pepper noise[4]. Following this, we performed skull-stripping using (https://github.com/HumanBrainED/NHP-BrainExtraction)[5]. Deepbet is a U-Net based deep learning tool which leverages a transfer-learning framework from a larger cohort of human imaging data and then retrained for brain extraction in NHPs to facilitate brain extraction of NHP data. This architecture allows for further retraining to account for differences in scanning acquisition, image quality, and animal age, requiring minimal retraining data and computational time in order to generalize models for new datasets. Deepbet includes models previously trained on a subset of data from the PRIME-DE and 136 masks generated for the first release of PRIME-DE data. In our study, we first applied the model 'Site-All-T-epoch_36_update_with_Site_6_plus_7-epoch_09' provided in Deepbet—which was initially trained on 19 macaques across 13 sites—as the starting model for generating brain masks for our data. When this model performed inadequately, we retrained it using manually corrected the failed masks of 2-3 scans from the same site to improve the performance. This approach was often iterative, requiring visual inspection, correction and retraining steps for specific sites where the initial model's generalizability was limited. Figure **S2.1.1-1** shows masks of four example datasets spanning infant and adult macaque scans. From this process brain masks were successfully created for all T1w images. T2w images within the same session were co-registered using rigid-body transformation to the T1w image to ensure consistent brain masks. For sessions with more than one scan, we created masks for the first scan and used rigid-body registration to align all subsequent scans with the first scan. After alignment, multiple scans within a session were averaged for further preprocessing. All masks generated for the T1w images data from PRIME-DE have been shared on GitHub: https://github.com/HumanBrainED/PRIME-Preprocessed/releases/tag/v0.1_anat_brainmask.

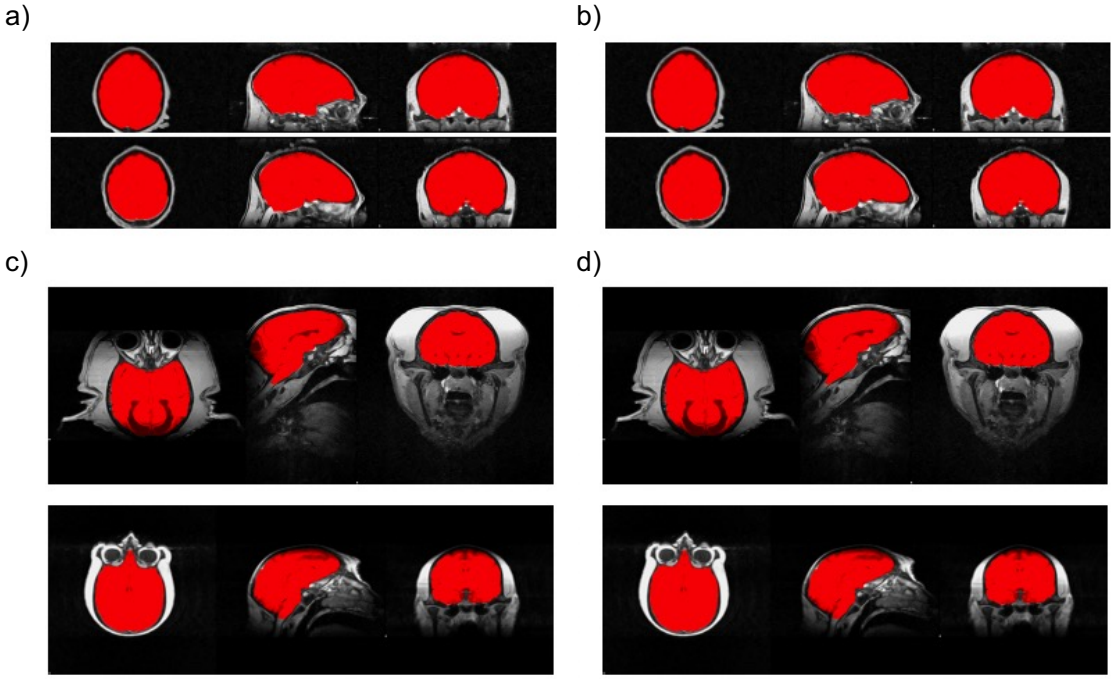

Fig. S2.1.1-1 | Example of brain extraction of Deepbet on data from four unique sites, spanning infancy (a, b) to adulthood (c, d). Each panel depicts two unique subject from a subset of sites: a) site-ucdavis-2, b) site-neurodev, c) site-emory, d) site-sbri.

2.1.2 Segmentation and Surface Reconstruction

With the brain mask generated, the T1w and T2w images were further preprocessed using the HCP-style macaque preprocessing pipeline 'nhp-abcd-bids-pipeline'[6–8]. Briefly, the pipeline includes anterior-posterior commissural (AC-PC) alignment, bias field correction, linear and nonlinear registration to the MacaqueYerkes19 template[7], tissue segmentation for gray matter, white matter, and subcortical regions, and surface reconstruction[6]. The pipeline was customized for NHP data, particularly for the segmentation and surface reconstruction steps[6–8].

To improve segmentation, the Joint Label Fusion approach was carried out using Advanced Normalization Tools (ANTs)[9]. In this approach, multiple annotated atlases are non-linearly registered to the target image (i.e. individual T1w images). Each atlas contributes to the labeling of the target image, weighted by its similarity between the deformed atlas and the target. By jointly considering all atlases during the label fusion step, a weighted voting process generates the final label of the target image. The atlases used as a joint label council were customized for rhesus macaques using a set of manually segmented images in the common template space in the HCP-style NHP preprocessing pipeline 'nhp-abcd-bids-pipeline'[6–8]. The default council included annotated segmentations from the Yerkes19 template along with nine segmentations created from macaques aged 4 months to 3 years, which was effective for most scans with an age older than 4 months. In total, 92.6% of 1,405 scans from animals older than 4 months successfully passed preprocessing and quality control. However, this default council does not accurately represent infant data, due to the ongoing process of myelination during the early developmental stage and differences in intensity contrast in T1w and T2w

images compared to adult macaques. To address this issue, we further customized the council by adding additional manually segmented animals from this infant age range. Overall, the inclusion of these additional segmentations improved the accuracy of the segmentation process for younger animals. To ensure the quality of the segmentation for infant data (age < 4 months), we conducted another round of visual inspections and performed manual corrections to fix minor errors. In total, 34 infant scans were corrected and passed the preprocessing and quality control (Section 2.2).

Surface reconstruction was performed using FreeSurfer v5.3.0[10]. Specifically, the data was scaled up by a factor of two, converting into a 'fake' space where the original 0.5 mm resolution was interpreted as 1 mm in FreeSurfer. Using the gray and white matter segmentation, the while and pial surfaces were reconstructed. Subsequently, the volume and surface data were reverted to the original size. The middle surface (midthickness) was then estimated by averaging the white and pial surfaces. The native surfaces were registered and resampled to the MacaqueYerkes19 template. To assess the quality of the surface reconstruction, the Euler Index was calculated (Section **S2.2.2**). Additionally, a visual inspection was carried out to ensure the accuracy of the surface reconstruction (Section **S2.2.1**). After quality control, 1,522 out of 1,860 scans (81.8%) successfully passed all preprocessing steps.

2.2. Quality Control (QC)

To ensure data quality, visual inspections were performed on the raw data received from collaborators, the organized BIDS formatted data downloaded from the PRIME-DE, as well as at each stage of the preprocessing pipeline. For the raw data, quality control involved visually inspecting the incoming anatomical images for discrepancies in orientation, metadata accuracy, and any evident abnormalities. The data was meticulously checked and corrected before converting into BIDS format and proceeding with preprocessing.

2.2.1 Visual Inspection

During MRI preprocessing, QC visual inspection images were generated for each step. The QC images for volumetric preprocessing steps, including brain extraction, segmentation, and registration, consist of multiple slices in the axial, coronal, and sagittal views. For the surface reconstruction, QC images include the snapshots of segmentation, gray-white matter boundaries overlaying the T1w image, and white and pial surface maps (**Fig. S2.2.1-1**). The QC images were rated on a scale from '1' (pass), '2' (small error), and '3' (bad) by three raters: SA, JR, and ZXW. The discordant ratings were reviewed and discussed with senior expert TX to reach a final consensus.

In brain extraction steps, we manually corrected some data rated with 'small error' or 'bad' to retrain the brain extraction model within site. Following this, we reran the model on the data rated 2-3 to assess whether their brain masks were improved. This process was repeated iteratively until all brain masks were successfully generated. For the segmentation and surface-reconstruction, QC images were first rated for all 1,861 scans. Data from infant macaques (age < 4 month) proved particularly challenging, with a failed example rated as a 3 shown in **Fig. S2.2.1-1**. To improve segmentation, we employed a customized joint label council in the preprocessing pipeline. The resulting segmentation rated as '2' was manually edited and reprocessed through the pipeline for surface reconstruction. Visual inspections

were conducted iteratively. Finally, data rated '1' were included in the final analyses, with data rated a score of 2 or 3 (i.e. labeled as 'fail' in **Fig. S2.2.1-2**) being excluded, resulting in 1,522 out of 1,861 scans. **Fig. S2.2.1-2** demonstrates the distribution of the 'pass' and 'fail' ratings.

a)

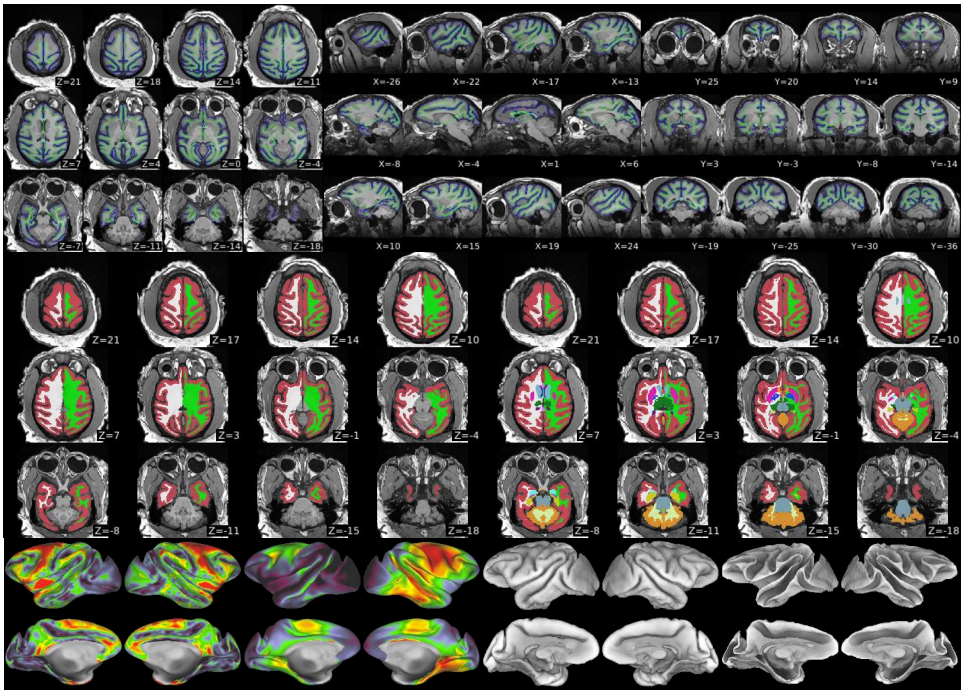

b)

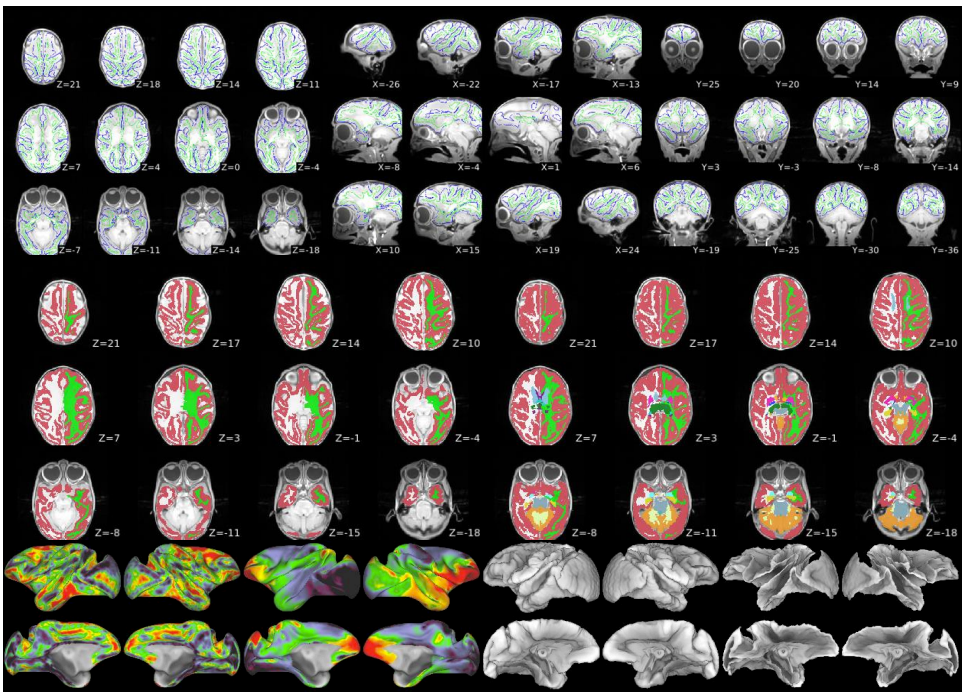

Fig. S2.2.1-1 | Example visual inspections of segmentation and surface reconstruction. **a)** A successful case with gray-white matter delineation, subcortical segmentation, and surface reconstruction. **b)** A 'bad' case with poor quality of data, segmentation and surface reconstruction.

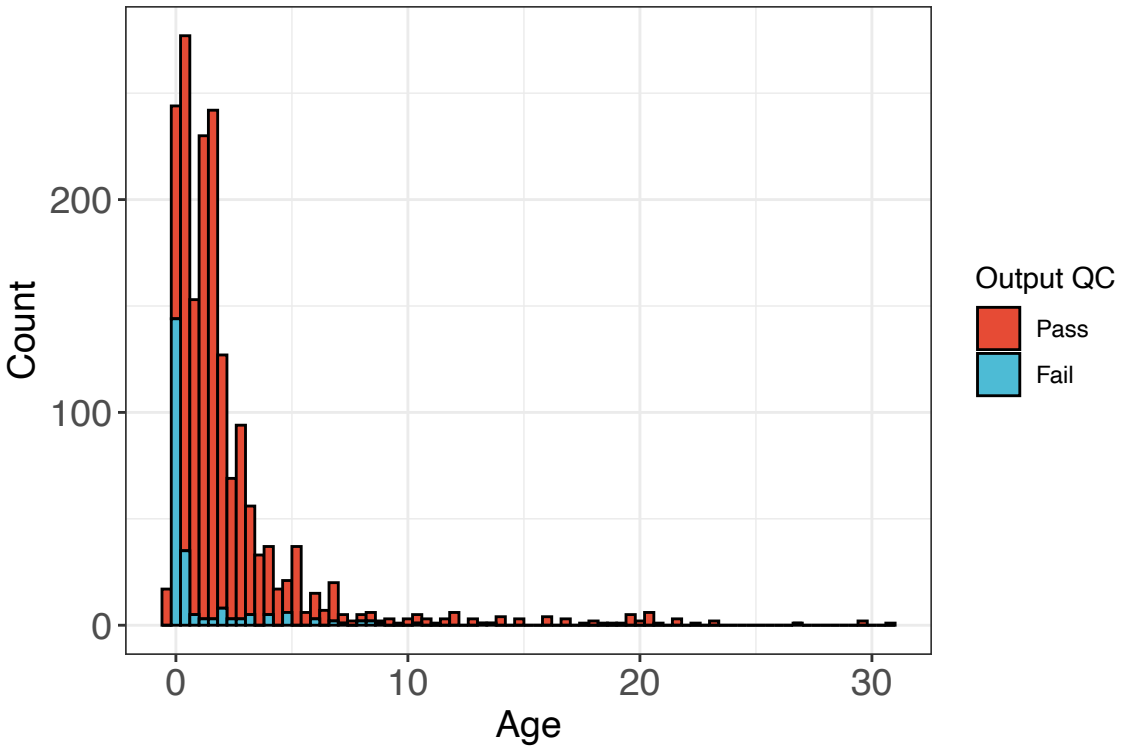

Fig. S2.2.1-2 | Distribution of 'pass' and 'fail' ratings across the aggregate dataset.

2.2.2 Euler Index

In addition to visual inspection, we examined the Euler Index (EI) to assess its impact on estimating the modeled brain development trajectories. The EI metric was calculated and extracted from the FreeSurfer pipeline which characterizes the topological complexity of the initial surface. Specifically, it summarizes the number of 'holes' or topological defects in the surface reconstruction[10]. **Fig. S2.2.2-1** shows the EI scores for each study site, revealing that the EI is generally consistent across research sites. No significant relationship was detected in EI among 17 study sites (ANOVA, $F_{502,16}$=1.127 p=0.326), with the exception of site-oxford, site-sbri, site-uwmadison, site-ucdavis-2, and site-ucdavis-3. We also examined the relationship between age variability and EI variability (**Fig. S2.2.2-2**), finding negligible correlations for both male (r=0.148) and female (r=0.168). Notably, several scans had susceptible high EI scores. Therefore, we further examined the impact of the EI's on the development models by comparing the EI with the centile scores estimated from GAMLSS (**Fig. S2.2.2-3**). The Spearman correlations between EI and centile scores were negligible across all four cerebrum tissue volumes (GMV: r=-0.17, sGMV: r=-0.14, WMV: r=0.09, Ventricles: r=0.03).

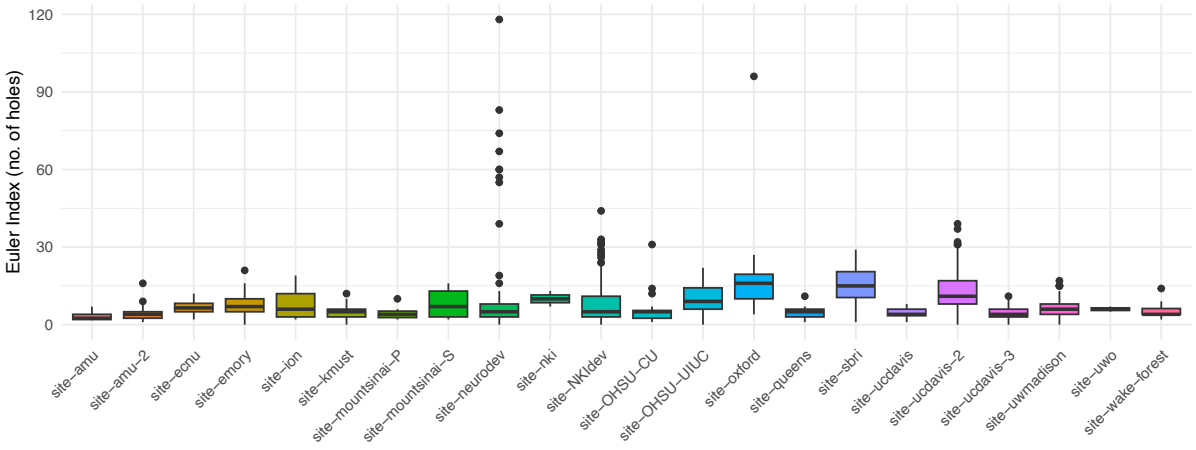

Fig. S2.2.2-1 | Euler Indices by study site. Boxplot shows the distribution of Euler Index for each site.

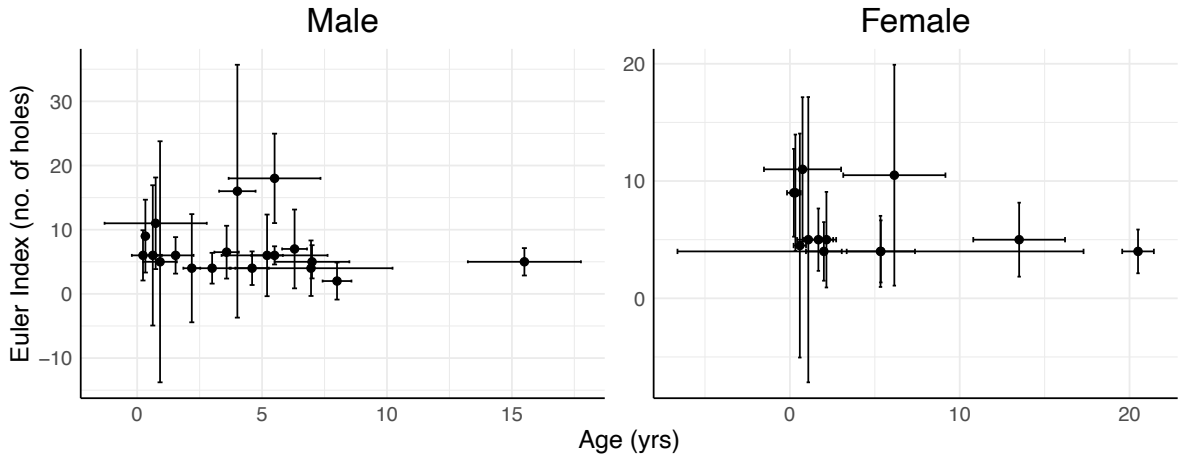

Fig. S2.2.2-2 | Age-related variability in image quality measured by the Euler Index. Black dots represent the median age (x-axis) and median EI (y-axis) for each study site (Male: left panel; Female: right panel). Crosshairs along the x-axis indicate the standard deviation of age per site, while crosshairs along the y-axis represent standard deviation of EI per site. The relationship between Euler Index and age was negligible for male (ρ=0.148) and female (ρ=0.168).

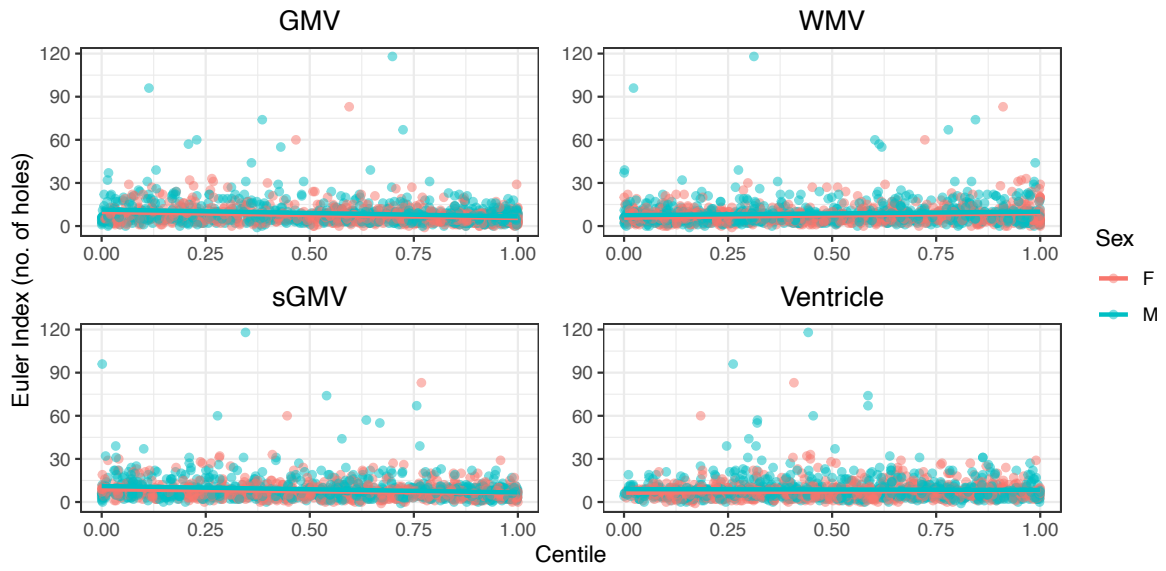

Fig. S2.2.2-3 | EI scores of each scan over centile distributions for four global tissue types. Spearman correlations between Euler Index and centile scores are negligible (GMV, ρ=0.17; WMV, ρ=-0.09, sGMV, ρ=0.14, Ventricle, ρ=-0.02).

2.3 Data Harmonization

In this study, all postnatal data was preprocessed using a standardized pipeline within a container on the same high-performance computing system. However, to improve segmentation accuracy for infant data (< 4 months), where the default pipeline was insufficient, we customized the segmentation step by incorporating additional infant-specific atlases into the joint-label fusion templates. Minor segmentation errors were further corrected through manual editing (**Section 2.1.2**). Due to differences in tissue segmentation step in preprocessing pipeline, we applied an additional batch harmonization step. For this subset of data (N=34, 2.2% of total scans), batch correction was performed using ComBat[11]. In alignment with previous study on human brain development, we also modeled site-specific datasets as a random effect in the GAMLSS framework to account for between-site heterogeneity. Of note, the prenatal data, which were derived from a single study with a small sample size, were included into the GAMLSS model to account for batch correction, rather than using ComBat[11]. This approach was chosen to prevent potential confounds between age and batch effects during early development. The specific procedures are detailed below.

2.3.1 ComBat Batch Correction

Customized infant atlases and manual correction was applied to a subset of data (rated as '2-3' score in QC during initial preprocessing) for infants below the age of 4 months. To mitigate potential discrepancies in tissue segmentation introduced by these adjustments, we performed batch correction to harmonize the global and regional volume, surface area, and cortical thickness. This was accomplished using the *'ComBat'*[11] function in R package 'sva' (version 3.46.0) with sex included as a covariate in the model. To avoid potential batch correction and confounds of the age effect, data was harmonized specifically within the 0 to 4 month age range. **Fig. S2.3.1-1** illustrates the distribution of the scans that were preprocessed

with the adjusted infant-specific atlases. **Fig. S2.3.1-2** presents pre-harmonized estimates of the global measurements color-coded by segmentation variation, with some noticeable differences in tissue estimation for WMV. **Fig. S2.3.1-3** shows tissue segmentation estimations post-ComBat harmonization with final median trajectories overlaid. The GAMLSS model fits on the final ComBat-harmonized data more clearly and adequately fits the dataset.

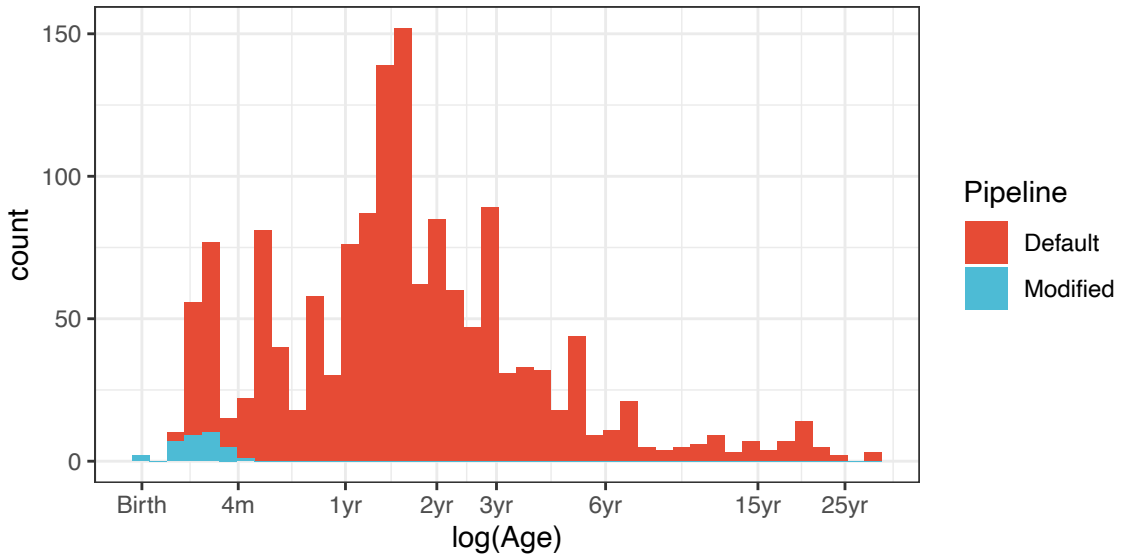

Fig. S2.3.1-1 | Distribution of scans processed with the standard or 'modified' pipeline. Modified pipeline used infant-specific segmentation atlases and additional manual correction.

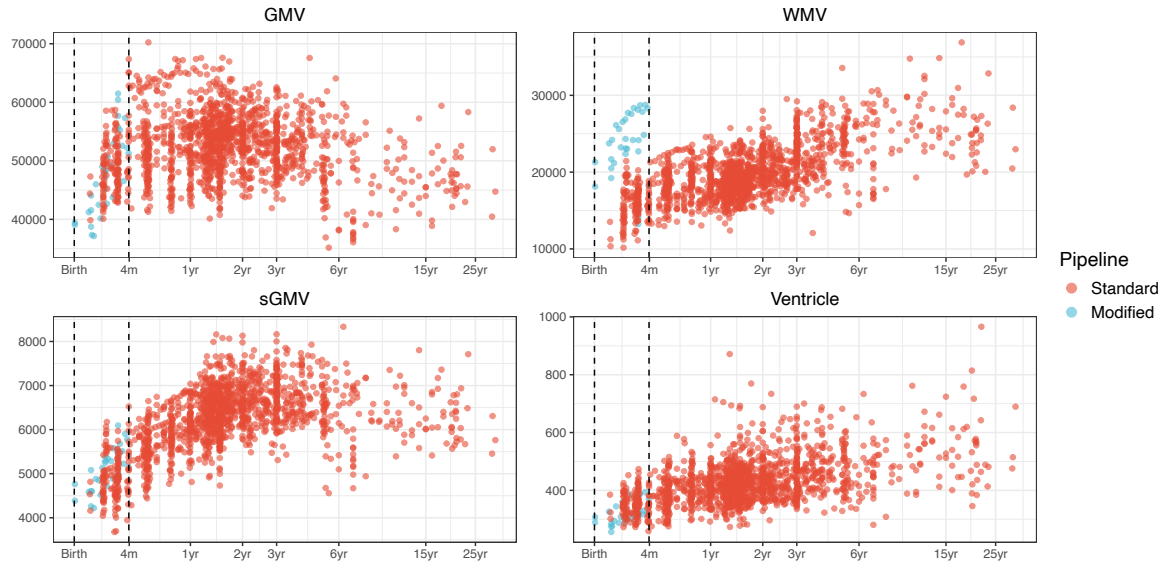

Fig. S2.3.1-2 | 'Raw' measurements before data harmonization, colored by pipeline variation. Scans within the dotted lines interval scans were harmonized. Noticeable differences, particularly for white matter volume are observed between standard and modified pipeline.

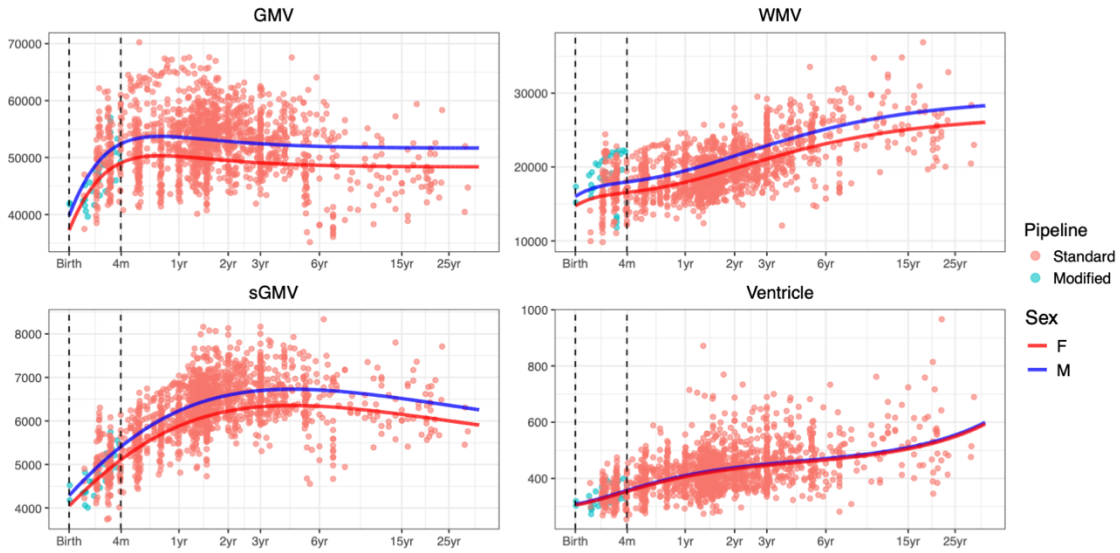

Fig. S2.3.1-3 | ComBat corrected data colored by pipeline variation with the resulting GAMLSS curves for male and female.

2.3.2 Evaluation from an External Pipeline for Infant Data

To further assess whether the tissue segmentation from our preprocessing pipeline, which utilizes an adjusted infant template for the early development data, introduces any bias in estimating age effects, we applied an additional pipeline[12] to the same infant dataset from site-neurodev. **Fig. S2.3.2-1** compares the estimated total volume, surface area, and mean thickness between two pipelines. The correlations were relatively high (total cortical volume: r=0.83, surface area: r=0.88, cortical thickness: r=0.75), indicating that both pipelines achieved good reliability.

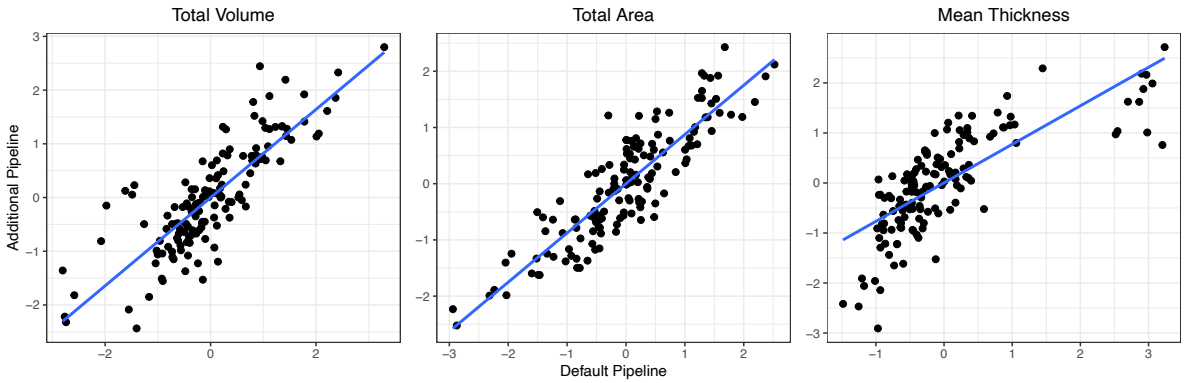

Fig. S2.3.2-1 | Between pipeline similarity of total cortical volume, surface area, and average cortical thickness of the same dataset (site-neurodev, N=160). X-axis indicates our 'default' preprocessing pipelines and y-axis indicates the additional pipeline from[12].

3. Model Evaluation

3.1 Model Diagnostics

Consistent with the previous study[2], we validated the model fits by examining the residuals of GAMLSS models from the four global tissue types to ensure goodness of fit. Specifically, we generated Detrended Transformed Owen's plots and traditional Quantile-Quantile (Q-Q) residual plots for each tissue type. Owen's plot is a general diagnostic tool in regression analysis used to visually assess the distribution of a fitted model. It is recommended for testing the adequacy of the model and guiding the selection of an appropriate distribution from a broad range of available distributions within a flexible GAMLSS framework[13,14]. In Owen's plot, we expect the confidence interval to include the zero-horizontal line; otherwise, it suggests the parametric distribution model is inadequate. **Fig. S3.1-1** illustrates that the model residuals for GMV, WMV, sGMV, and ventricles were normally distributed, supporting the adequacy of the fitted generalized gamma distributions.

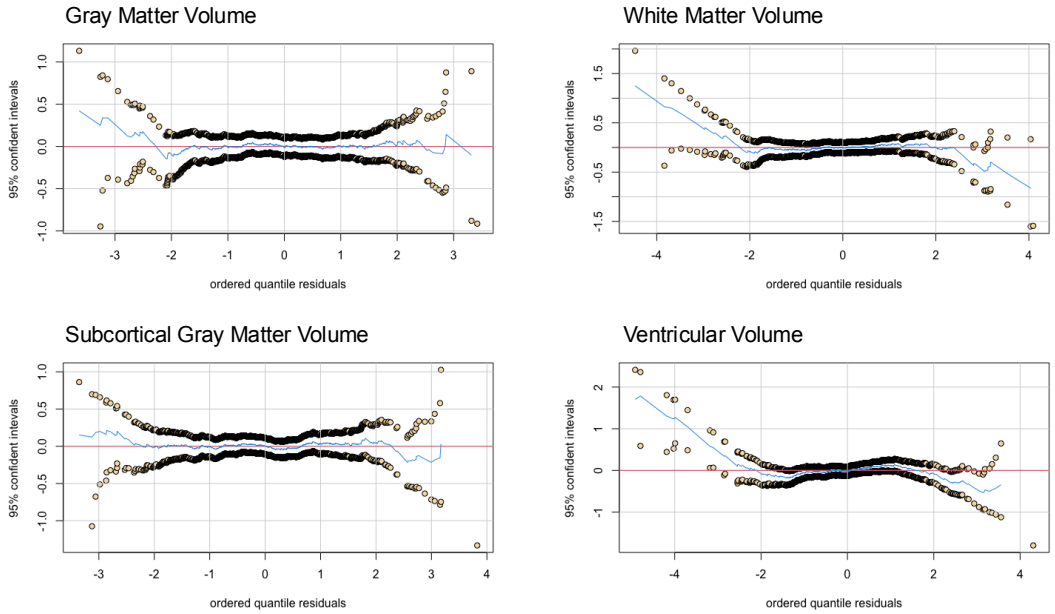

Fig. S3.1-1 | Detrended Transformed Owen's plots of model residuals. Visual inspection of residuals showes that the zero-horizontal line is mostly within the confidence interval for four global phenotypes, indicating the adequacy of the fitted distributions.

In addition, we also visualized the standard Q-Q plots for each tissue type. Q-Q plots compare the quantiles of the theoretical distribution with those of the sample data. When the residuals follow the reference line closely, it indicates that they are normally distributed, suggesting that the model fits the data well. **Fig. S3.1-2** shows the Q-Q plots for GMV, WMV, sGMV, and ventricles. The residuals visually appear to align with the reference line for each global tissue type (GMV: skewness = 2.021e-05, kurtosis = 3.049, Filliben coefficient = 0.999, WMV: skewness = -0.003, kurtosis = 3.872, Filliben coefficient = 0.996, sGMV: skewness = 0.008, kurtosis = 3.165, Filliben coefficient = 0.999, and ventricle volume: skewness = 0.0008, kurtosis = 4.56, Filliben = 0.992).

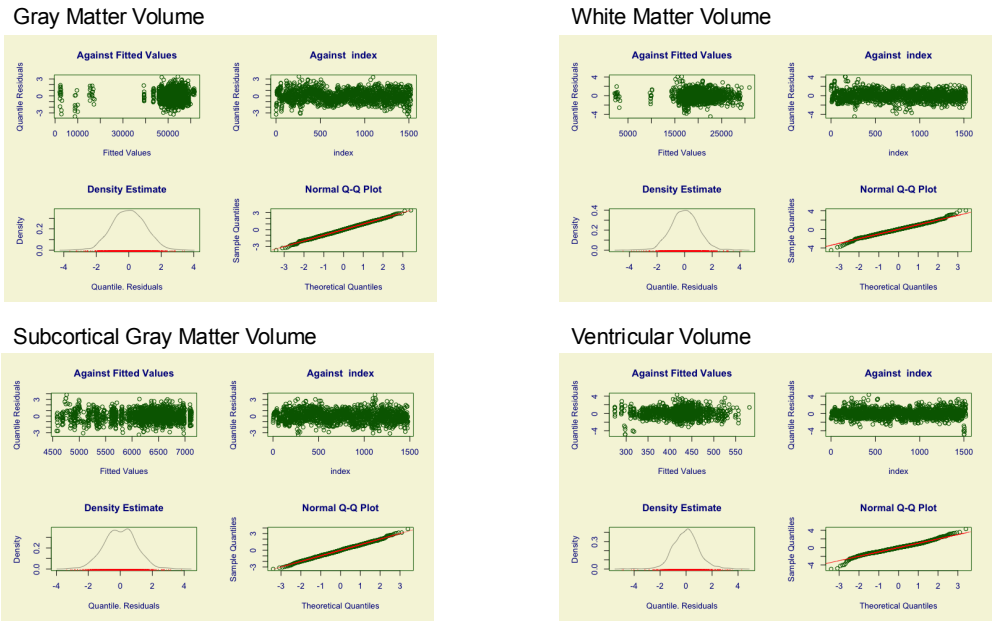

Fig. S3.1-2 | Q-Q plots for the four global brain phenotypes. Plots suggest residuals are normally distributed for Gray Matter Volume (skewness = 2.021e-05, kurtosis = 3.049, Filliben coefficient = 0.999), Cortical White Matter Volume (skewness = -0.003, kurtosis = 3.872, Filliben coefficient = 0.996), SubCortical Gray Matter Volume (skewness = 0.008, kurtosis = 3.165, Filliben coefficient = 0.999), and Ventricular Volume (skewness = 0.0008, kurtosis = 4.56, Filliben = 0.992), supporting the adequacy of fitted distributions

3.2 Bootstrapping Analysis

To assess model stability for GAMLSS fits for trajectory parameters estimated for both global and regional phenotypes, we conducted 1,000 bootstrap iterations of the fitting procedure with stratified resampling with replacement. This allows us to derive confidence intervals of all GAMLSS fits and parameter estimates, including normative trajectories, centiled trajectories, and site-specific μ effects. **Fig. S3.2-1** shows normative trajectories for each of the four global volumes and their corresponding confidence intervals. Overall, the confidence "ribbons" of the trajectories were relatively narrow across the lifespan, particularly for GMV and WMV. Greater variance was observed in the early and late stages of life for ventricular volume and subcortical gray matter volume. This variability is likely due to the limited data available for these age ranges, as most of our dataset covers animals aged between 6 months to 6 years. Additionally, subcortical regions in MRI data are commonly noisier with low signal-to-noise ratio compared to gray matter and white matter contrast. Therefore, the segmentation of sGMV and ventricular volume tend to be less stable.

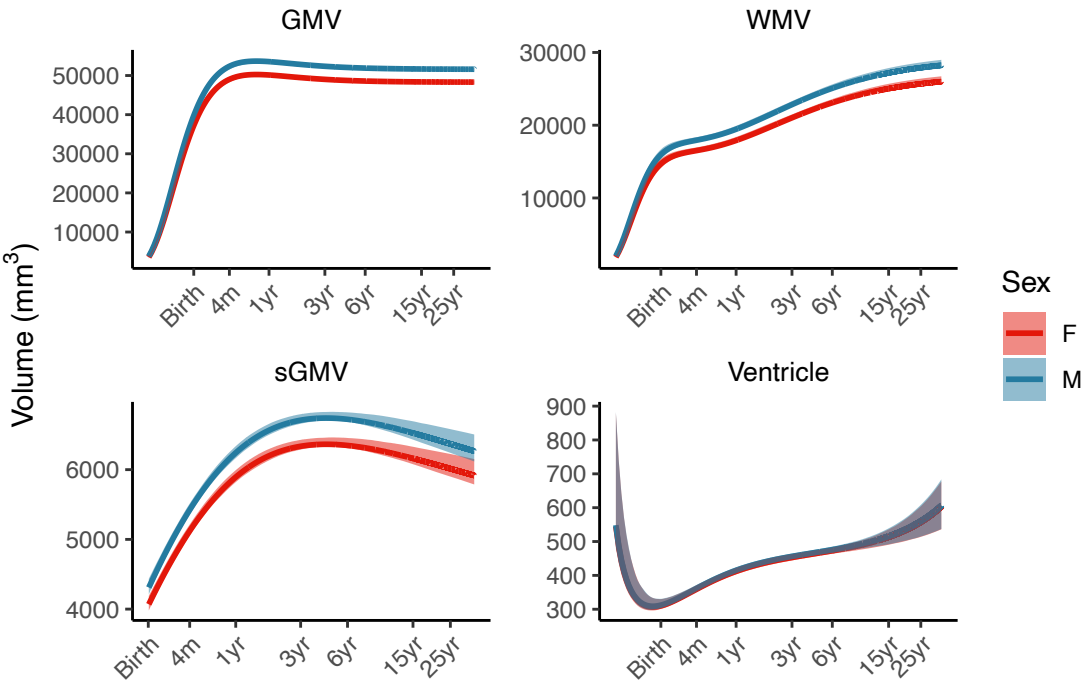

Fig. S3.2-1 | Normative trajectories with boostrapped confidence intervals for four global brain phenotypes. Shaded ribbons indicate 95% confidence intervals calculated across 1,000 sex-stratified bootstrapping resampling with replacement. Sex-balance is perserved in each resampling iteration. Four global phenotypes are total gray matter volume (GMV), total white matter volume (WMV), subcortical gray matter volume (sGMV), and ventricular volume.

3.3 Parameter Estimations

We also calculated confidence intervals of model parameters (i.e. μ) from the 1,000 bootstrapping procedure of GAMLSS for each study site. Confidence intervals with relatively narrow ranges for the GAMLSS parameter μ indicate a stable estimation for a specific site. In our GAMLSS model, we incorporated site-specific random effects. **Fig. S3.3-1** shows the offset of the μ estimation and bootstrapped 95% confidence intervals. The average site-specific μ is colored by the average age of scans per site. In general, the confidence intervals are relatively narrow for all study sites, suggesting stable and robust estimation of μ in GAMLSS models.

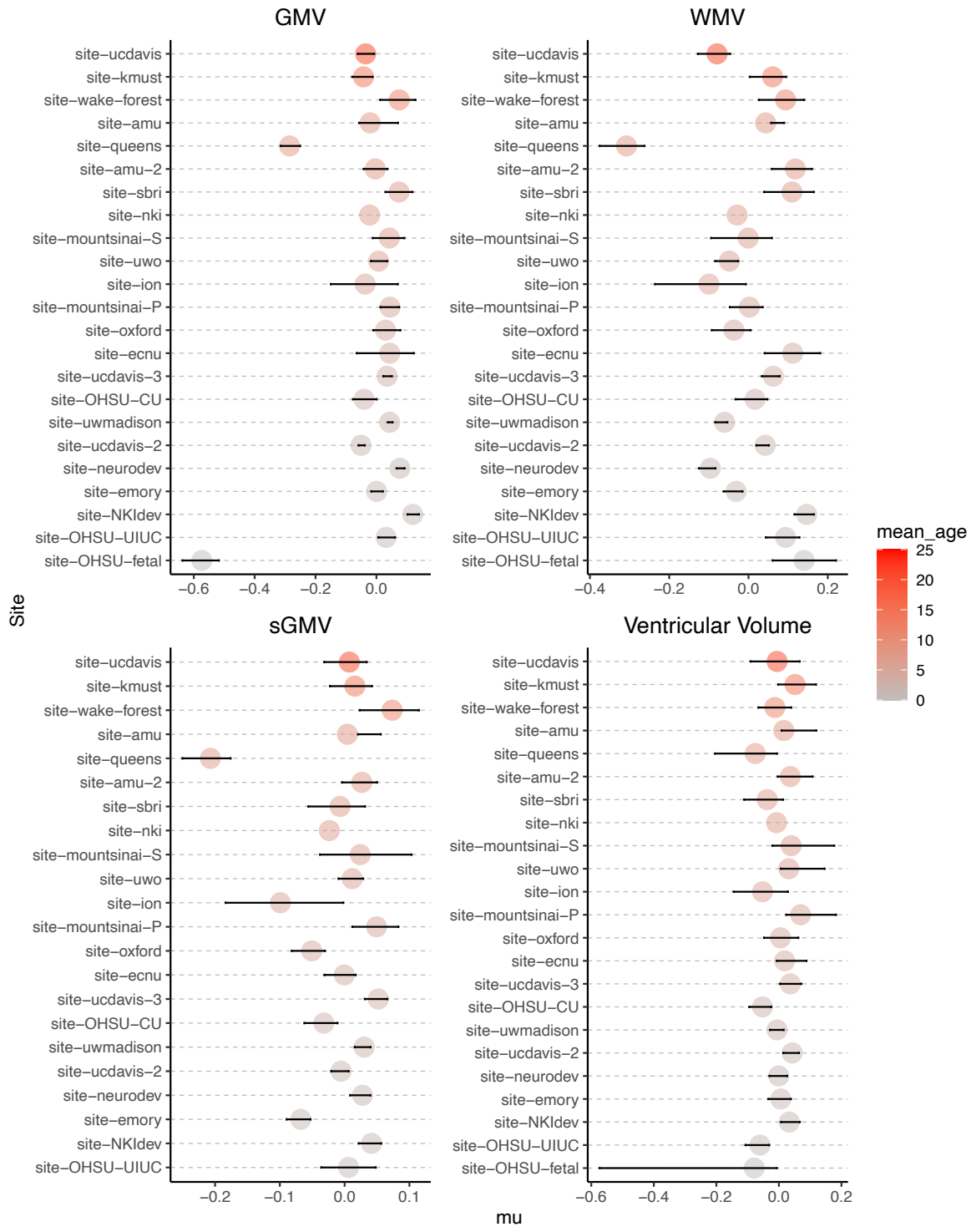

Fig. S3.3-1 | Site-specific random effects on estimation of μ with 95% confidence intervals across 1000 bootstrapping iterations. Study sites were sorted by average age of each site.

To test the extent to which the age effect is potentially driven by site-specific effects, we conducted regression models to investigate relationships between median age of each site and the resulting μ parameter. **Fig. S3.3-2** shows the average estimation of μ and median age for each site with their linearly fit curves. No significant effect was detected across all four global phenotypes (GMV: t=0.142, p=0.888; WMV: t=-1.075, p=0.295; sGMV: t=-0.121,

p=0.905; Ventricle: t=0.766, p=0.452). Similarly, we conducted regression to assess the effect for standard deviation of age and sample size on the μ for each site (**Fig. S3.3-3-S3.3-4**) with no significant effect observed either (GMV: t=0.788, p=0.440; WMV: t=0.810, p=0.427; sGMV: t=1.309, p=0.205; Ventricle: t=0.258, p=0.799) (GMV: t=0.021, p=0.983; WMV: t=0.327, p=0.747; sGMV: t=0.694, p=0.496; Ventricle: t=-0.174, p=0.863). This analysis confirmed that GAMLSS parameter estimates for site-specific effect μ are not influenced by the age distribution or sample size.

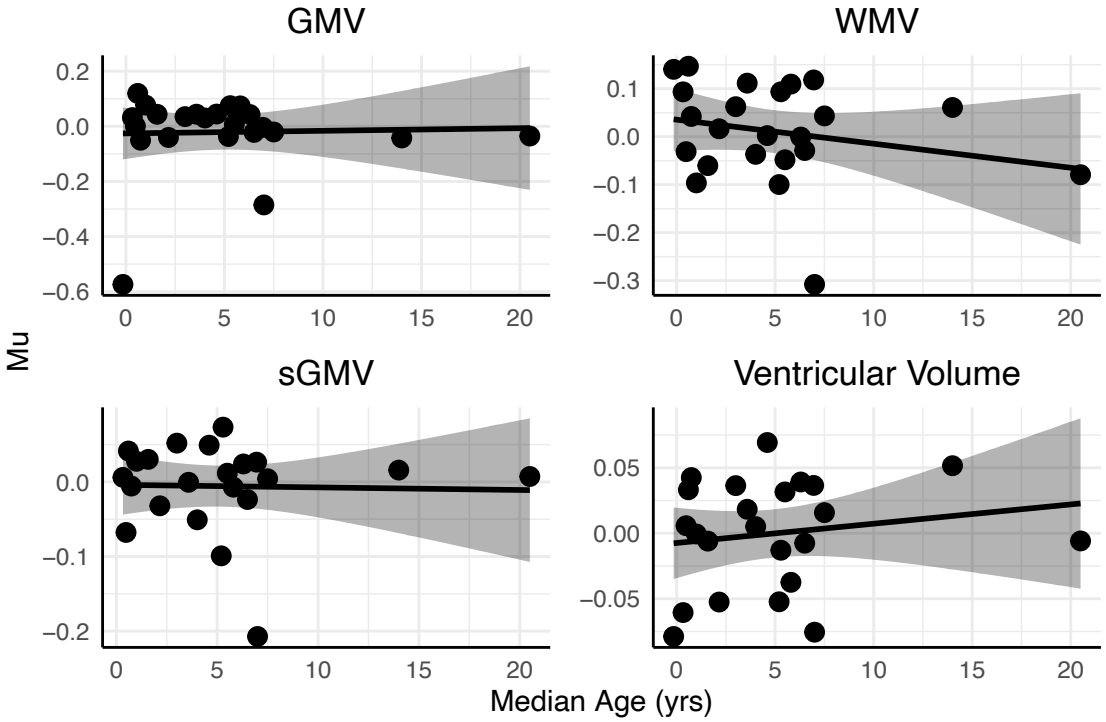

Fig. S3.3-2 | Linear model fits on the relationship between site random effect and median age by global metrics. Linear testing reveals no significant relationship between μ effect and age for any global phenotype (GMV: t=0.142, p=0.888; WMV: t=-1.075, p=0.295; sGMV: t=-0.121, p=0.905; Ventricle: t=0.766, p=0.452).

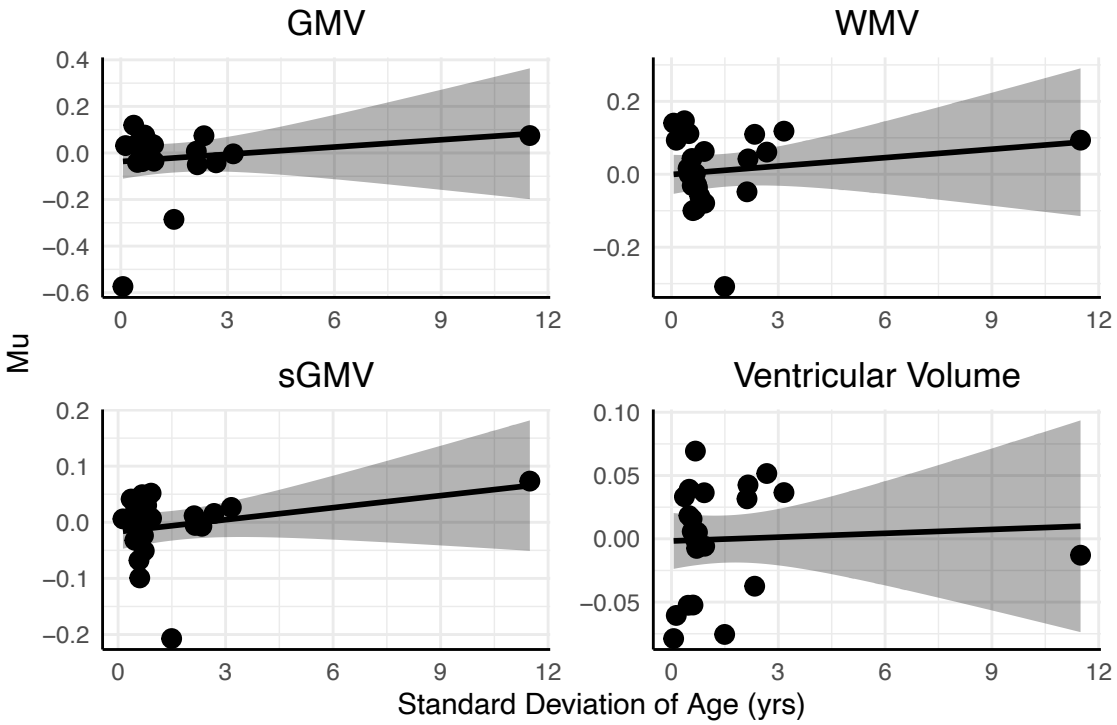

Fig. S3.3-3 | Scatterplots of μ intercept estimation over standard deviation of age, with linear model fits. No significant linear relationship between standard deviation of age and random effect parameters is present (GMV: t=0.788, p=0.440; WMV: t=0.810, p=0.427; sGMV: t=1.309, p=0.205; Ventricle: t=0.258, p=0.799).

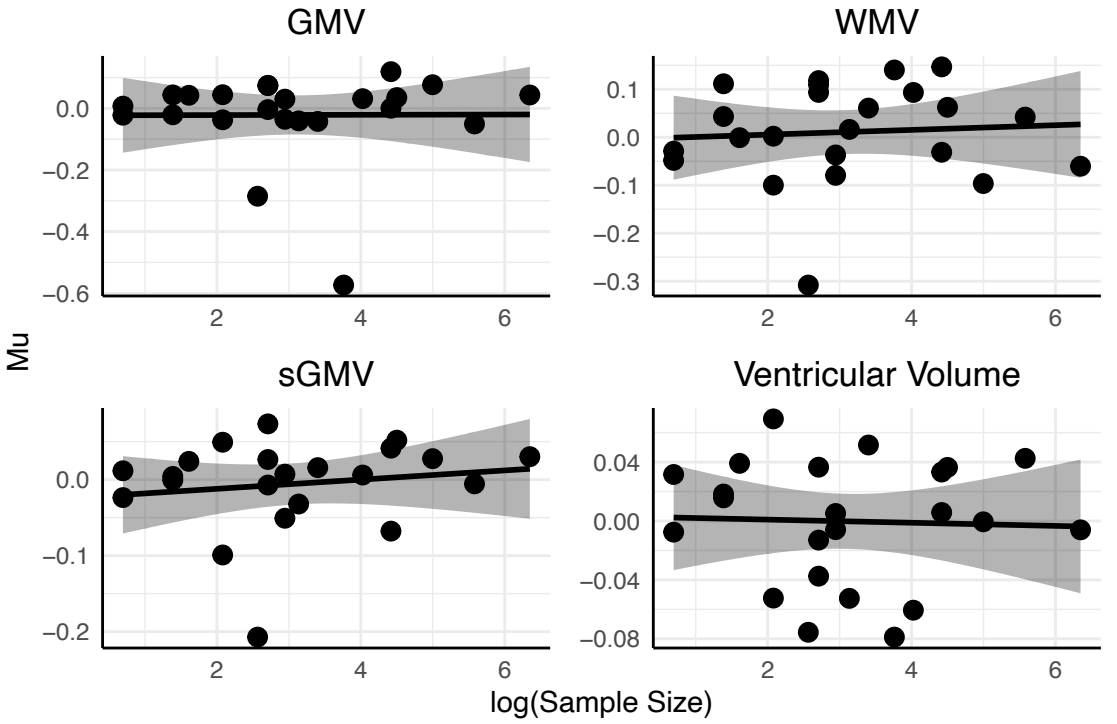

Fig. S3.3-4 | Scatterplots between site μ random effect and log sample size. Linear models reveal no significant relationship (GMV: t=0.021, p=0.983; WMV: t=0.327, p=0.747; sGMV: t=0.694, p=0.496; Ventricle: t=-0.174, p=0.863).

4. Developmental Trajectories and Milestones

Beyond the developmental charts for global phenotypes, we also modeled age-related trajectories for finer-grained cortical and subcortical regions. As with the global phenotypes, quality-controlled data were used for these analyses. **Fig. 4-1** shows the Markov parcellation applied to the cortical regions in the study, which defined 91 symmetric parcels across hemispheres. For each parcel, we extracted bilateral cortical volume, surface area, and mean thickness. Additionally, we extracted the volumes of the cerebellum and key subcortical regions, including the thalamus, amygdala, hippocampus, pallidum, and putamen. Notably, only postnatal data were available and included in the regional analyses. ComBat correction was first applied to the infant data, which were preprocessed using the default pipeline with an adjusted infant template. We used the same GAMLSS framework with fractional polynomial distributions to fit nonlinear, sex-stratified growth curves for regional measurements. The same model selection process was applied, with the optimal combination of fractional polynomial models for each region determined based on the BIC. To estimate confidence intervals for the model parameters, we performed 1,000 bootstrap resampling iterations on the original data. Finally, we identified the ages at which each regional measurement reached its maximum size (i.e., peak), as well as the corresponding growth rates (i.e., first derivative of the estimated growth curves).

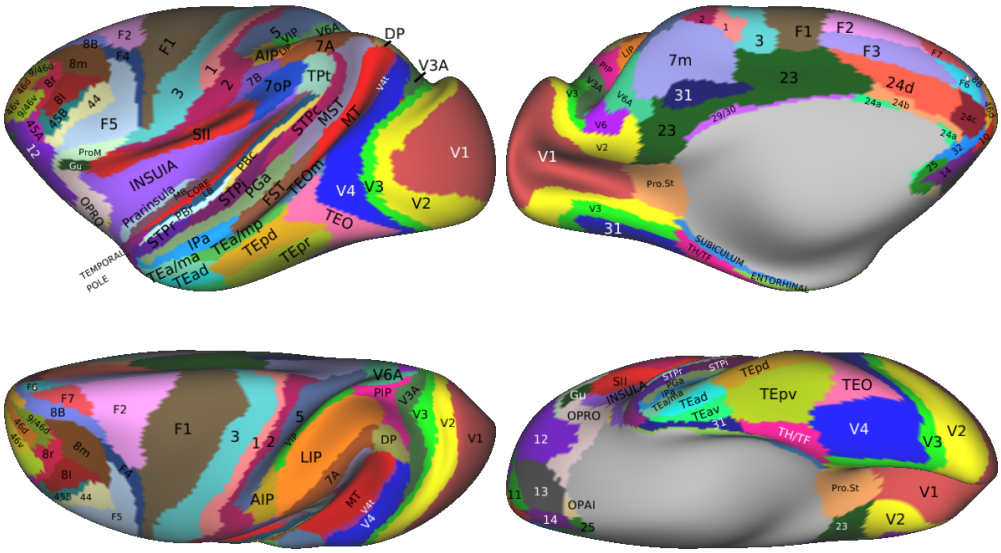

Fig. S4-1 | Markov parcellation and parcel annotations[3].

4.1 Regional Trajectories

In this section, we report the ComBat corrected data used in the GAMLSS models (**Fig. S4.1-1**, **S4.1-3**, **S4.1-6, S4.1-9**), the normative trajectories with 2.5% and 97.5% centiles (**Fig S4.1-2, S4.1-4, S4.1-7, S.4.1-10**), and the proportional scores at the key developmental milestones of the macaque lifespan, including birth, infancy (4 months), juvenility (1 year), adolescence (6 years), adulthood (15 years), and older age (25 years). Proportional scores were calculated by dividing the 50th centile estimate (i.e. median) of the GAMLSS trajectory (50th centile) by

the regional maximum at key developmental stages, stratified by sex (**Fig. S4.1-5, S4.1-8, S4.1-11**).

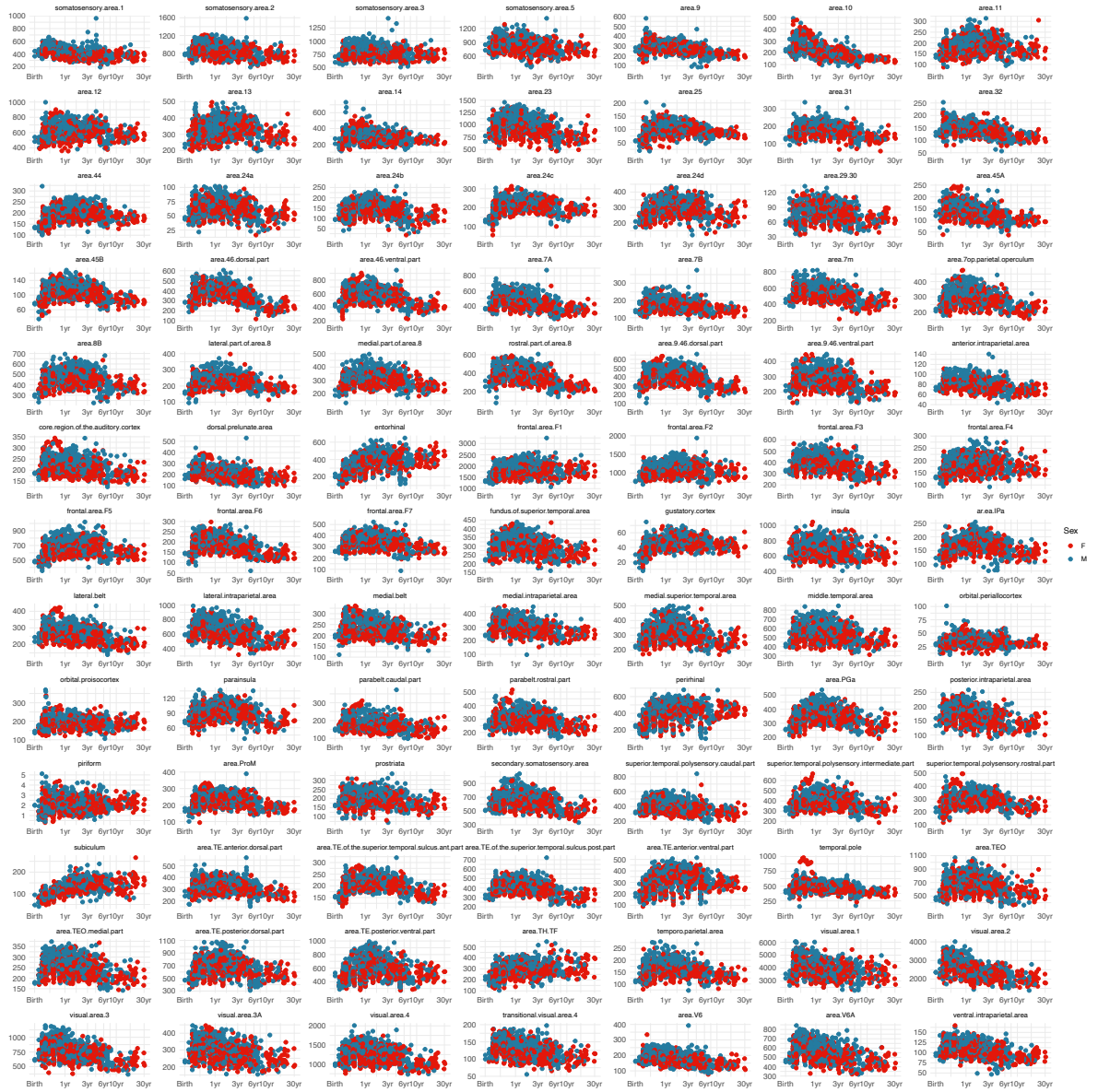

Fig. S4.1-1 | Regional volumetric (mm^3) data across lifespan for 91 bilateral cortical regions, as defined by the Markov parcellation[3].

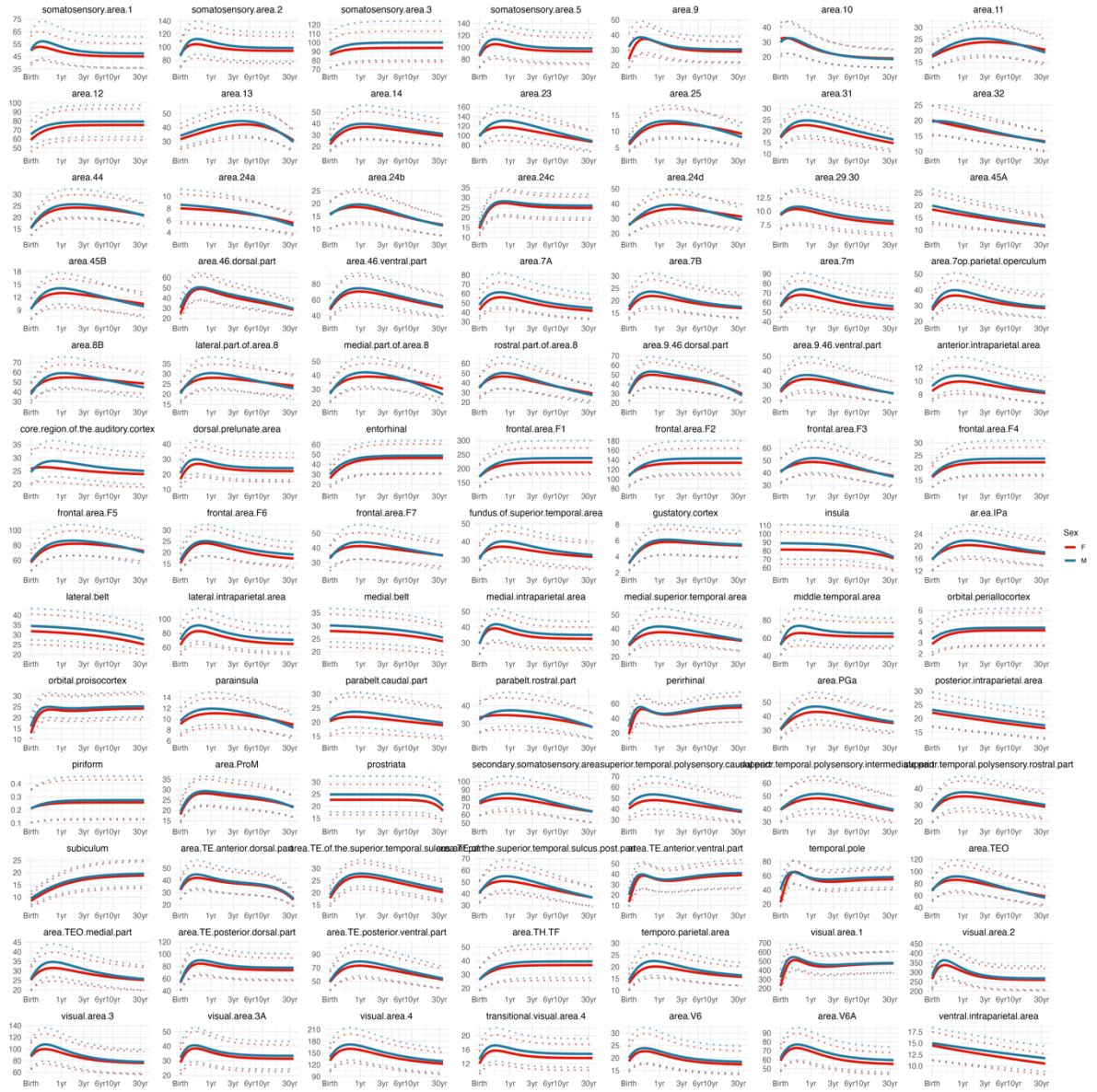

Fig. S4.1-2 | Normative trajectories of regional volume, with confidence intervals, were modeled across the lifespan for 91 bilateral cortical regions as defined by the Markov parcellation[3]. Dotted lines indicate the 2.5% and 97.5% centiles for each modeled region. These trajectories were fit from optimal models selected from the GAMLSS framework based on the data shown in **Fig. S4.1-1**, similar to the global trajectories shown in Fig 1.

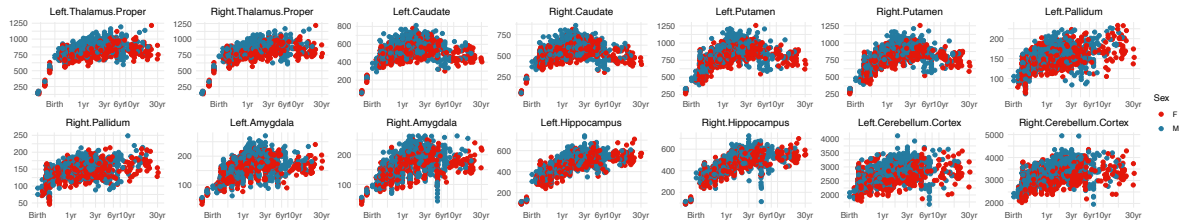

Fig. S4.1-3 | Regional volumetric (mm^3) data for cerebellum and subcortical regions, including the thalamus, caudate, putamen, pallidum, amygdala, and hippocampus.

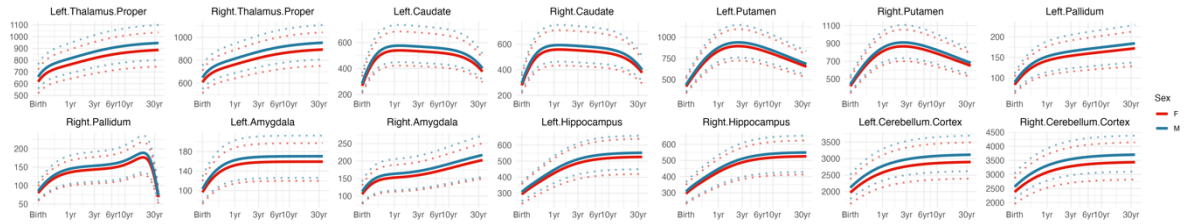

Fig. S4.1-4 | Normative trajectories of regional volume, with confidence intervals, were modeled across the lifespan for cerebellum and subcortical regions. Dotted lines indicate the 2.5% and 97.5% centile lines for each modeled region. These trajectories were fit from optimal models selected from the GAMLSS framework based on the data shown in **Fig. S4.1-3**, similar to the global trajectories shown in Fig 1.

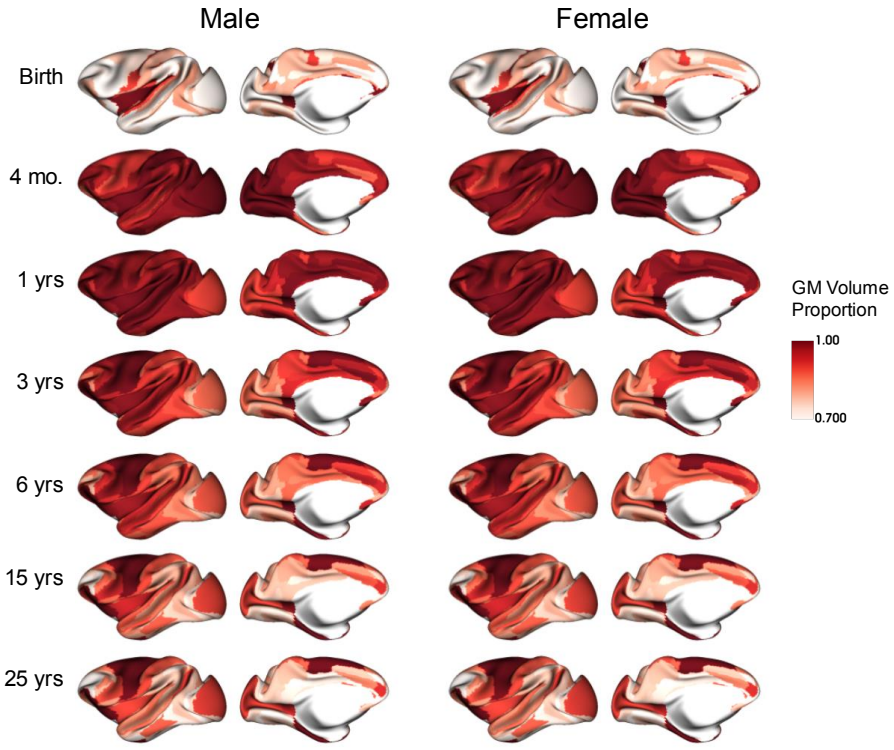

Fig. S4.1-5 | Regional volumetric proportional size (mm^3 / maximum) at key development milestones shown in Fig. 3. Proportional scores were calculated by dividing the 50th centile estimate of the trajectory by the regional maximum at key developmental stages across the macaque lifespan, including birth, infancy (0.33 years, or 4 months), childhood (1 year), juvenility (3 years), adolescence (6 years), adulthood (15 years), and older age (25 years).

Fig. S4.1-6 | Regional surface area (mm^2) data across lifespan for 91 bilateral cortical regions, as defined by the Markov parcellation[3].

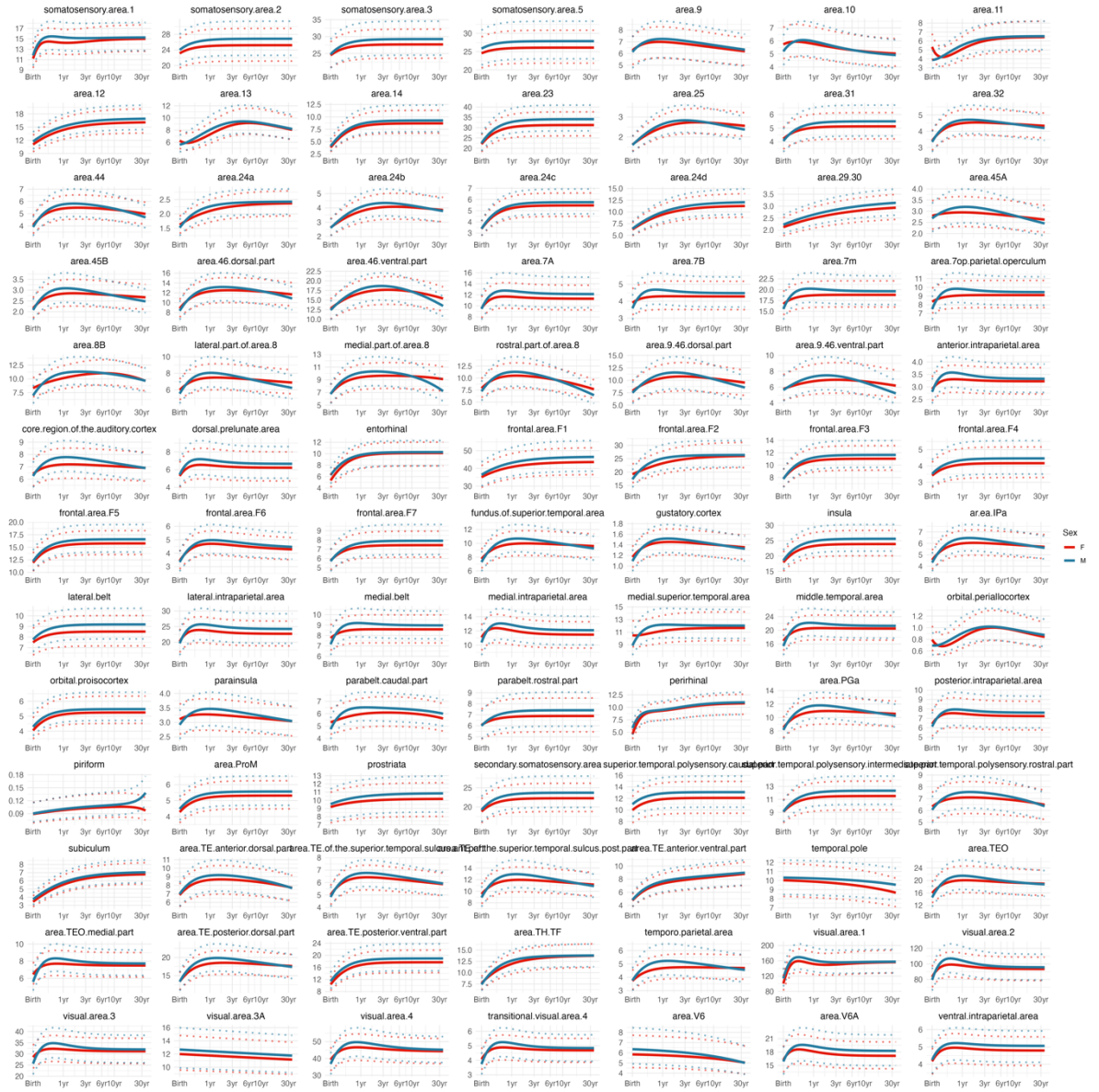

Fig. S4.1-7 | Normative trajectories of regional surface area, with confidence intervals, were modeled across the lifespan for 91 bilateral cortical regions as defined by the Markov parcellation[3]**.** Dotted lines indicate the 2.5% and 97.5% centiles for each modeled region. These trajectories were fit from optimal models selected from the GAMLSS framework based on the data shown in **S4.1-6**, similar to the global trajectories shown in Fig 1.

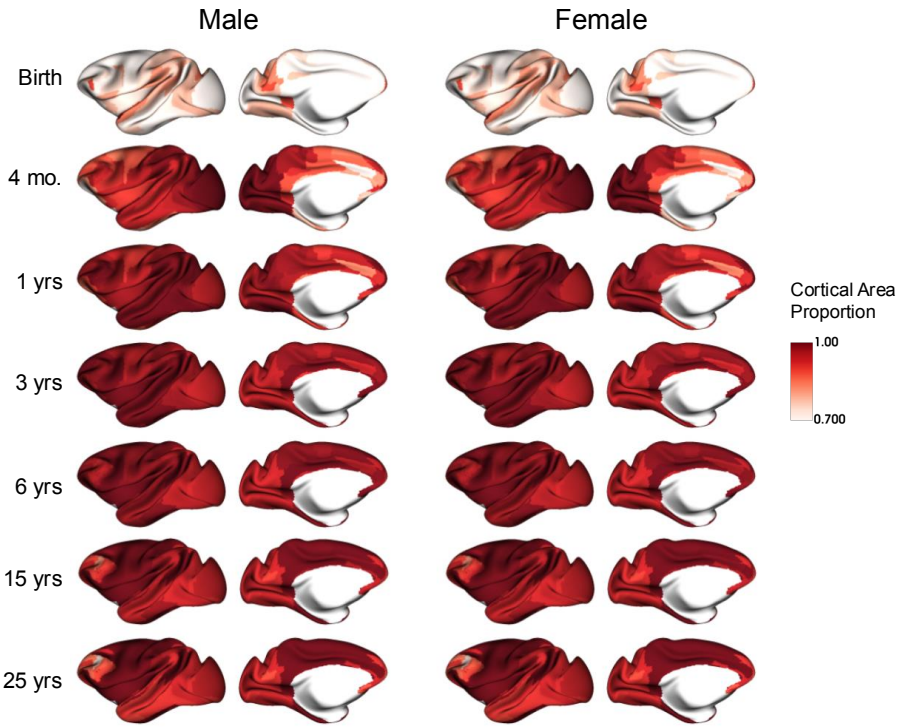

Fig. S4.1-8 | Regional areal proportional size (mm^2/maximum) at key development milestones shown in Fig. 3. Proportional scores were calculated by dividing the 50th centile estimate of the trajectory by the regional maximum at key developmental stages across the macaque lifespan, including birth, infancy (0.33 years, or 4 months), juvenility (1 year and 3 years), adolescence (6 years), adulthood (15 years), and older age (25 years).

Fig. S4.1-9 | Regional cortical thickness (mm) data across lifespan for 91 bilateral cortical regions, as defined by the Markov parcellation[3].

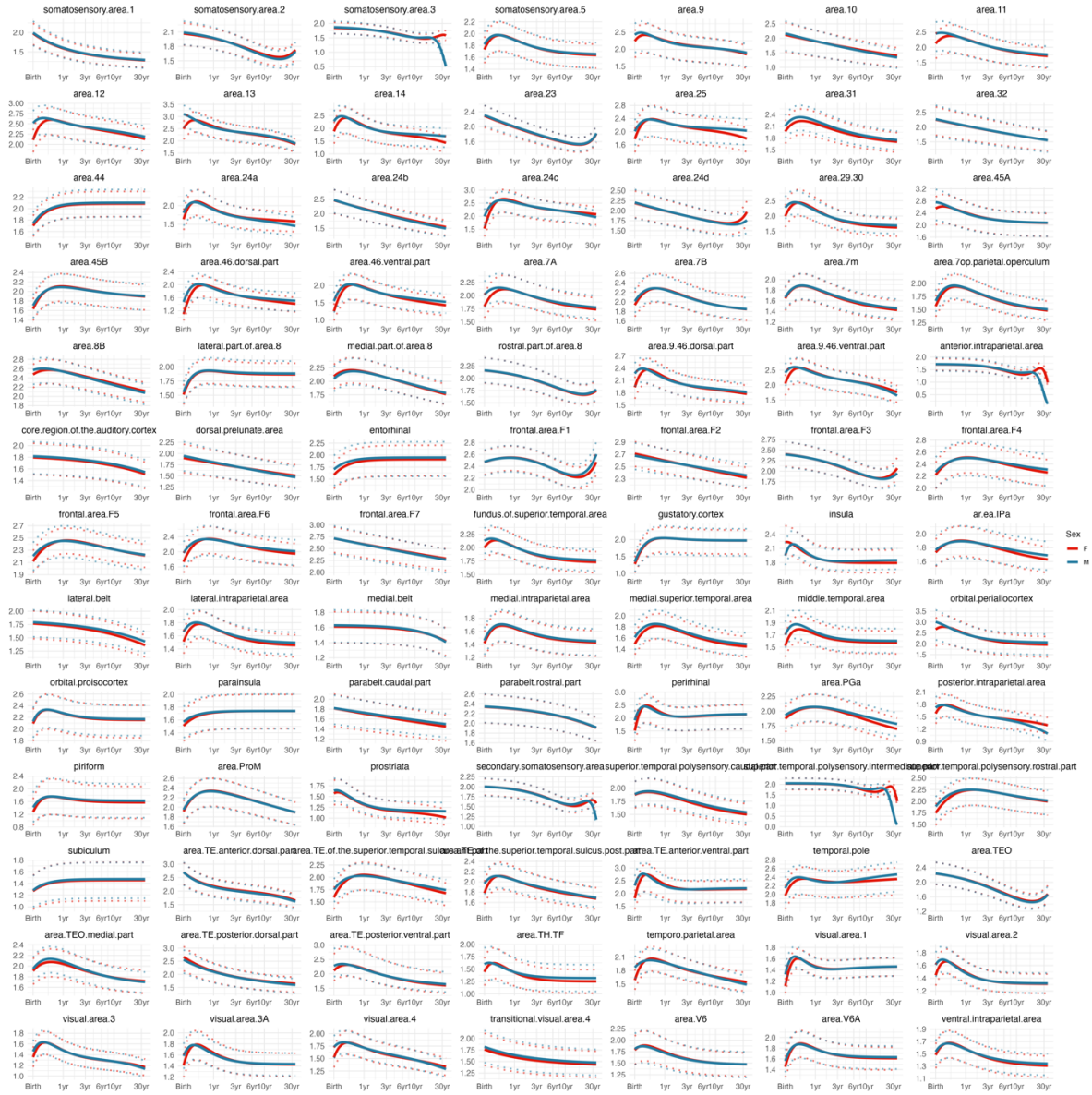

Fig. S4.1-10 | Normative trajectories of regional cortical thickness, with confidence intervals, were modeled across the lifespan for 91 bilateral cortical regions as defined by the Markov parcellation[3]. Dotted lines indicate the 2.5% and 97.5% centiles for each modeled region. These trajectories were fit from optimal models selected from the GAMLSS framework based on the data shown in **Fig. 4.1-9**, similar to the global trajectories shown in **Fig 1**.

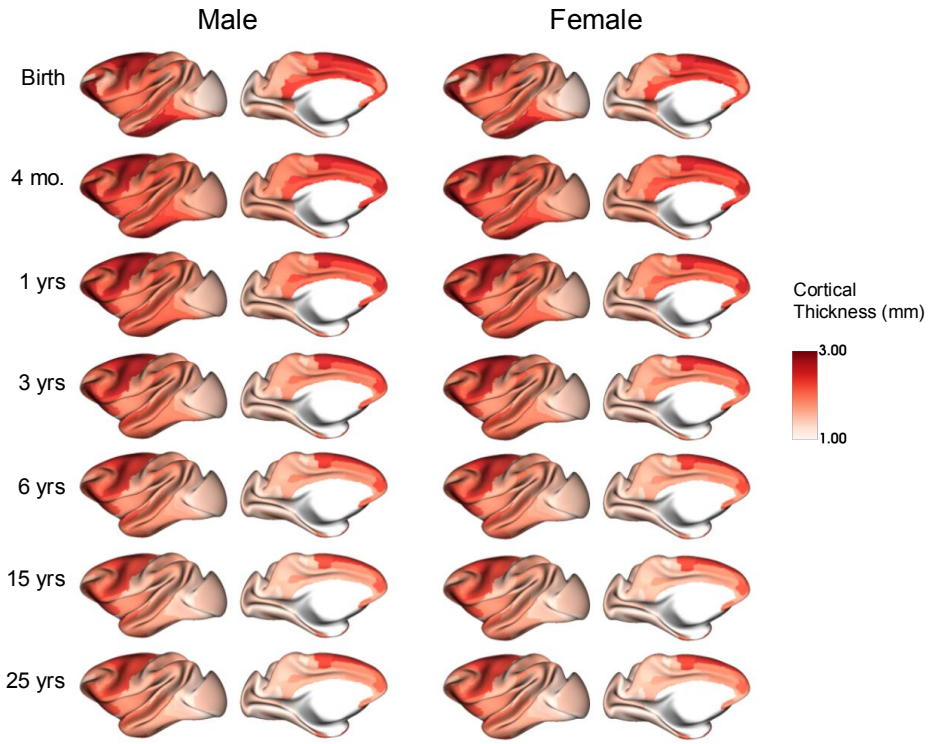

Fig. S4.1-11 | Regional cortical thickness (mm) at key development milestones shown in Fig. 3. Milestones include birth, infancy (0.33 years, or 4 months), juvenility (1 year and 3 years), adolescence (6 years), adulthood (15 years), and older age (25 years).

4.2 Regional Peak Age

In addition to the regional peak ages reported in Fig 2, we fit 1,000 bootstraps to estimate the confidence intervals for the peak ages of regional volume, surface area, and cortical thickness. Peak age was identified as the age at which the regional measurement plateaued (i.e., slope=0). For regions where the measurement approaches, but does not reach a true maximum, we defined the age at which the rate of change is nearly zero (i.e. slope < 0.05). **Fig. S4.2-1** ranks regions by their median peak age estimated in GAMLSS with the range of each point representing the 95% bootstrapped confidence intervals. Results showed that peak ages are relatively stable across bootstraps, with narrow 95% confidence interval ranges (volume: 0.26 ± 0.34 years, surface area: 1.01 ± 1.82 years, and mean thickness: 0.14 ± 0.15 years). These results underscore the robustness of the peak age estimation.

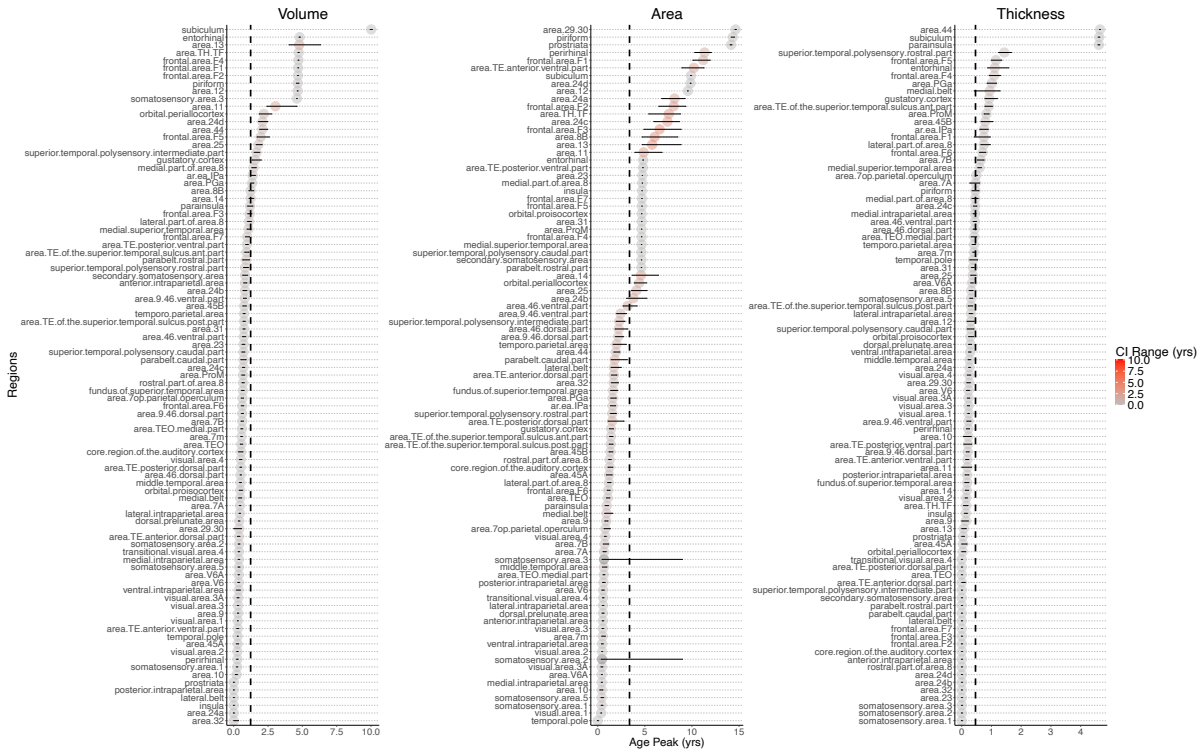

Fig. S4.2-1 | Regional peak age estimations with 95% bootstrapping confidence intervals of regional volume, surface area, and cortical thickness. Regions are ranked by peak age and colored by the range of 95% bootstrapped confidence intervals. Black, dashed line represents the average peak across all regions.

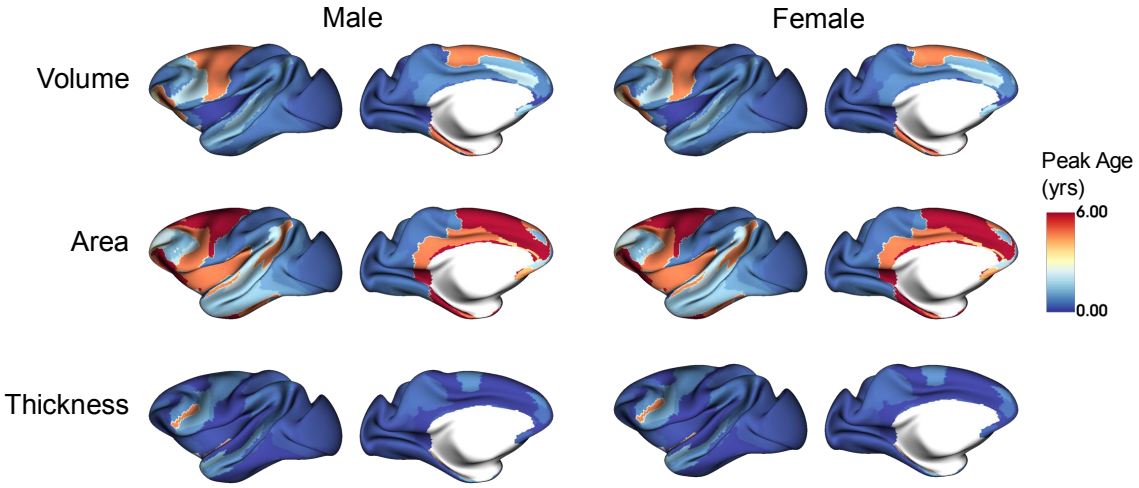

Fig. S4.2-2 | Regional peak age (in years) of bilateral regions for cortical gray matter volume, cortical surface area, and cortical thickness. Peak age was identified as the age at which the regional measurement plateaued (i.e., slope=0). For regions where the measurement approaches, but does not reach a true maximum, we define the age at which the rate of change is nearly zero (i.e. slope < 0.05).

4.3 Regional Growth Rate

We also estimated growth rates by calculating the first derivative of the 50th centile (i.e. median) trajectory from the GAMLSS models, representing the daily change (i.e. velocity) in regional volume (mm^3/day), surface area (mm^2/day), and cortical thickness (mm/day). **Fig. S4.3-1**, **S4.3-3**, and **S4.3-5** show the growth rate for each region individually. For both volume and surface area, growth rates were positive postnatally for most regions but decreased over time, indicating continued growth with a deceleration during development. In contrast, several regions of cortical thickness reached a plateau prenatally and exhibited negative growth rates after birth. Additionally, we visualized growth rates at key developmental milestones across the macaque lifespan—birth, infancy (4 months), childhood (1 year), juvenility (3 years), adolescence (6 years), adulthood (15 years), and older age (25 years), stratified by sex (**Fig S4.3-2, S4.3-4, S4.3-6**).

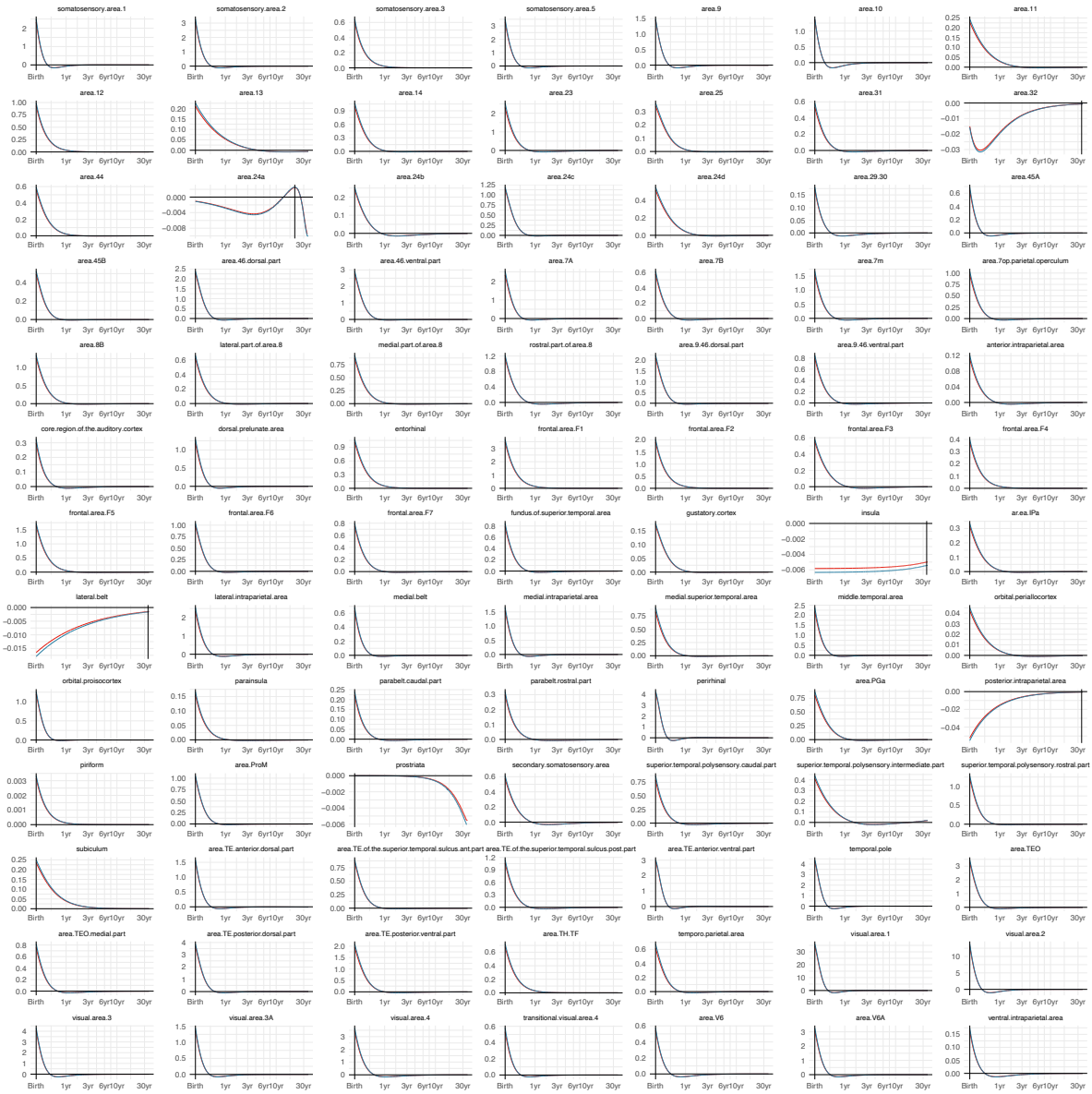

Fig. S4.3-1 | Rate of growth of regional volumes across the lifespan for 91 bilateral regions defined by the Markov parcellation[3]. Rate of growth calculation is estimated identically to the global metrics, as seen in Fig. 1 and Fig. 2 of the main text. Intersection of rate of growth lines with the horizontal line at *y=0* denotes peak maturity, while vertical lines intersect at peak rate of growth.

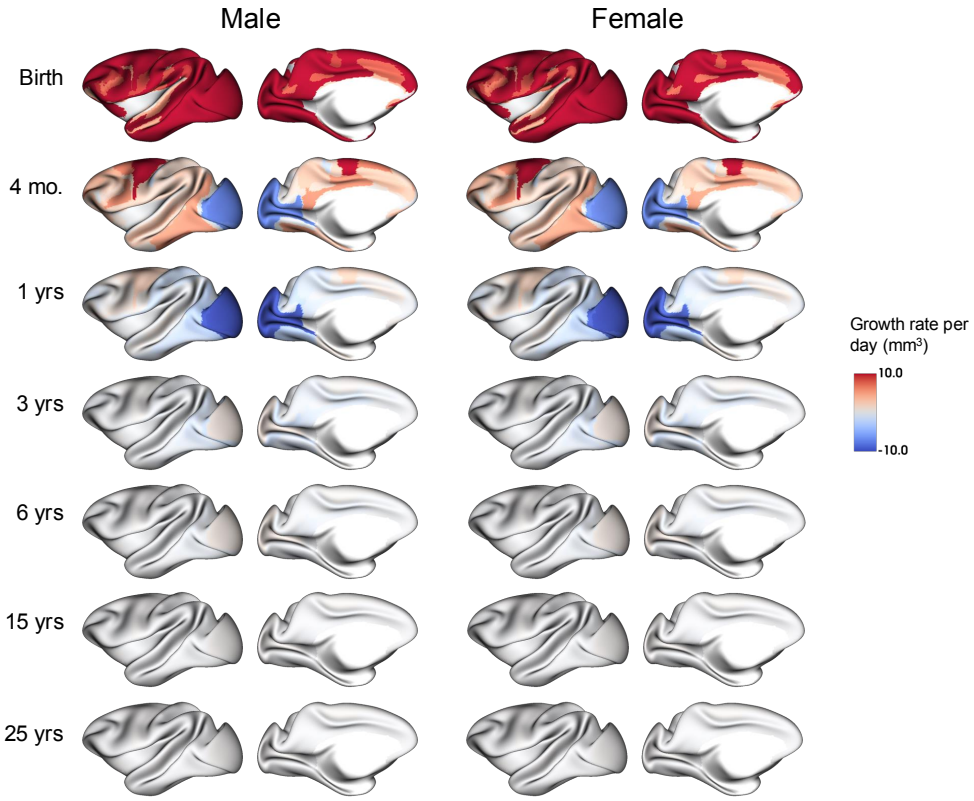

Fig. S4.3-2 | Growth rate of regional volumes (mm^3/day) at key developmental milestones, including birth, infancy (0.33 years, or 4 months), childhood (1 year), juvenility (3 years), adolescence (6 years), adulthood (15 years), and older age (25 years).

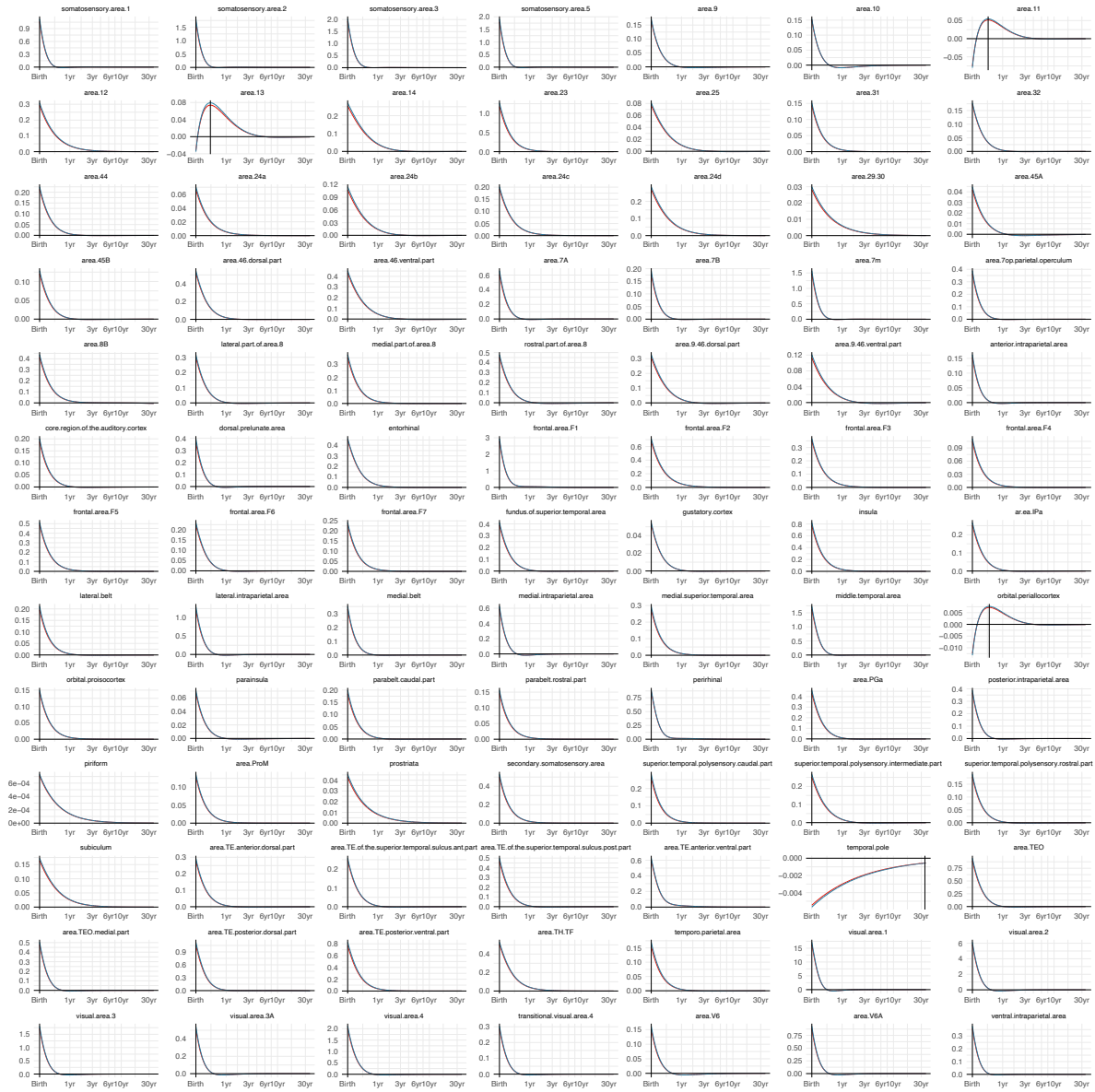

Fig. S4.3-3 | Rate of growth of regional surface areas across the lifespan for 91 bilateral regions defined by the Markov parcellation[3]. Rate of growth calculation was estimated identically to the global metrics, as seen in Fig. 1 and Fig. 2. Intersection of rate of growth lines with the horizontal line at *y=0* denotes peak maturity, while vertical lines intersect at peak rate of growth.

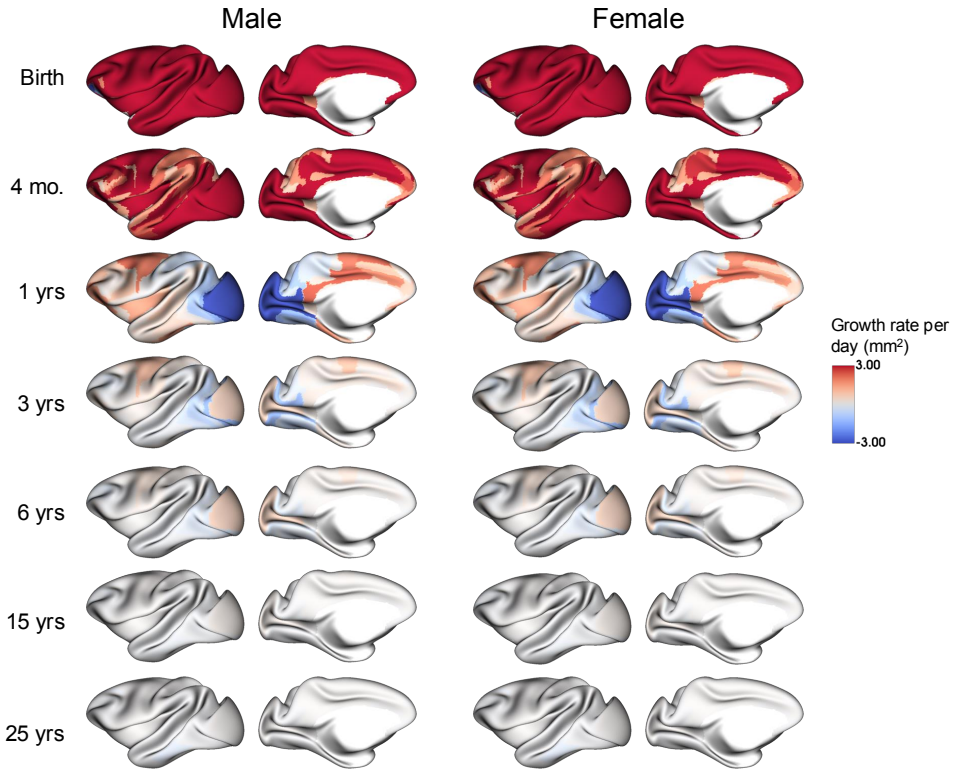

Fig. S4.3-4 | Growth rate of regional surface area (mm^2/day) at key developmental milestones, including birth, infancy (0.33 years, or 4 months), childhood (1 year), juvenility (3 years), adolescence (6 years), adulthood (15 years), and older age (25 years).

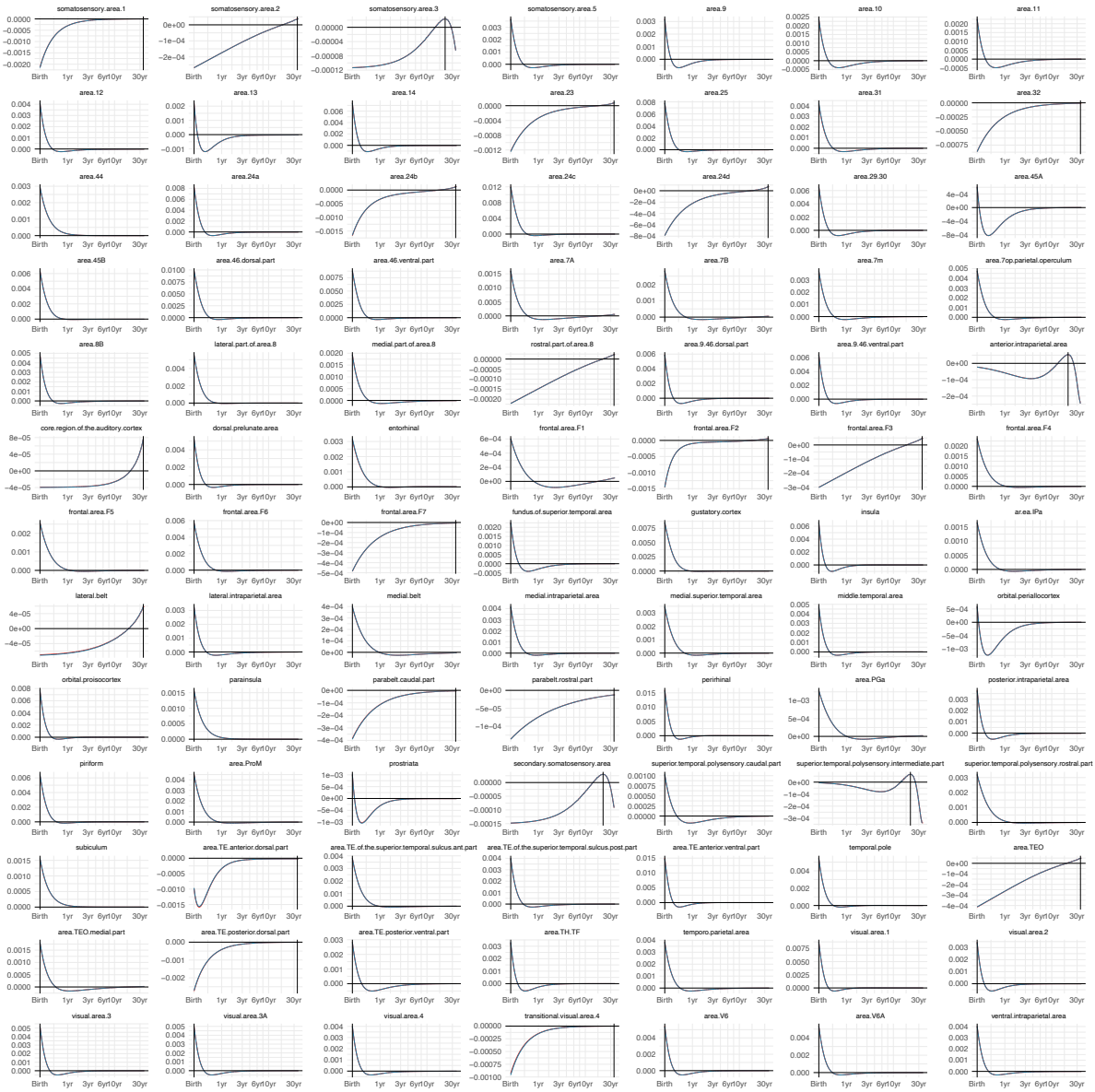

Fig. S4.3-5 | Rate of growth of regional cortical thickness across the lifespan for 91 bilateral regions defined by the Markov parcellation[3]. Rate of growth calculation was estimated identically to the global metrics, as seen in Fig. 1 and Fig. 2. Intersection of rate of growth lines with the horizontal line at *y=0* denotes peak maturity, while vertical lines intersect at peak rate of growth.

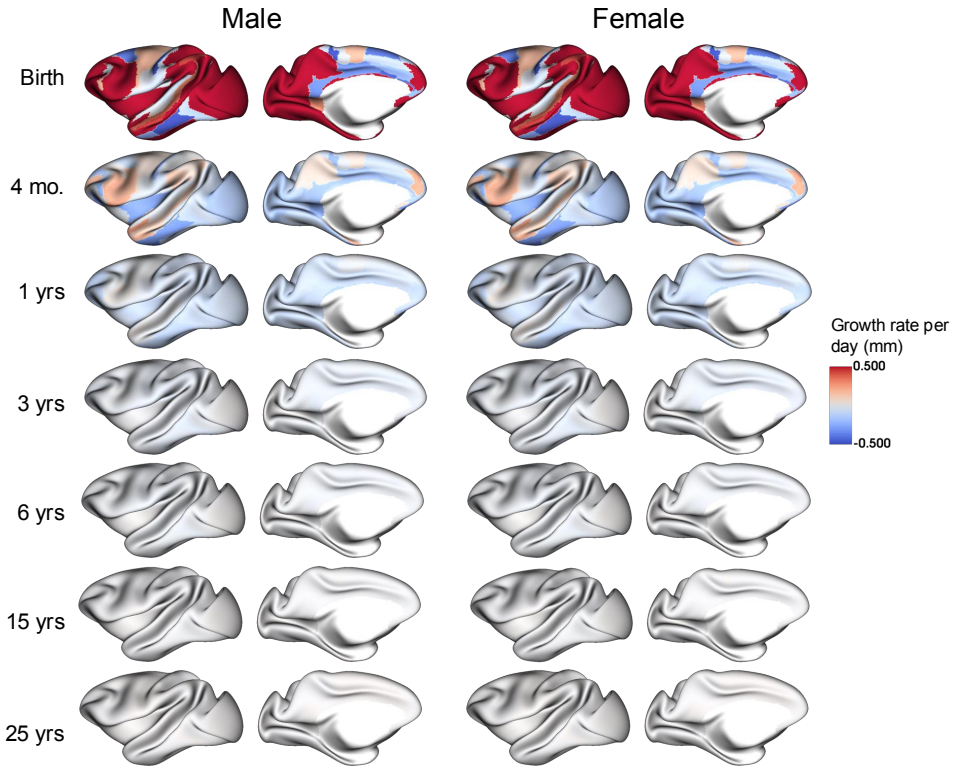

Fig. S4.3-6 | Growth rate of regional cortical thickness (mm^2/day) at key developmental milestones, including birth, infancy (0.33 years, or 4 months), childhood (1 year), juvenility (3 years), adolescence (6 years), adulthood (15 years), and older age (25 years).

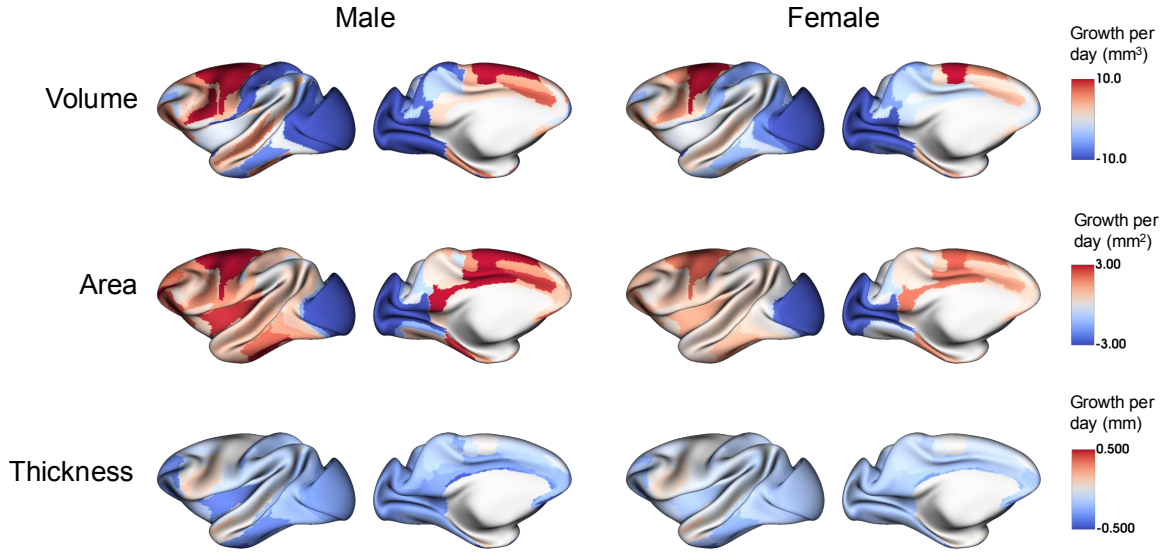

Fig. S4.3-7 | Regional growth rates for macaque at the age of peak total gray matter volume (0.74 years). Sex-stratified models were generated for bilateral averages of each region. Growth rates for male and female are shown on the left hemisphere for visualization (the left panel is identical to Fig 2d).

5. Neurosynth Meta-Analysis

To understand the associated cognitive development of brain growth, we performed a meta-analysis, decoding incremental, proportional volumetric growth maps over cognitive functions. Growth maps were calculated by taking regional changes in proportional volume in humans and macaques at 3 month and 1 month increments, respectively, from birth to adolescence (0-18 years for humans, 0-6 years for macaques). This resulted in 72 growth change maps for each species. Each map for humans were then correlated with activation maps of cognitive terms from the meta-analytical tool "Neurosynth"[15]. The macaque maps were first transformed into human space then decoded accordinally. All cognitive terms were categorized into a sets of 24 cognitive topics previously reported (e.g. "person", "empathy", "people" are grouped into the topic "social cognition")[16] (see Method).

To generate the cognition development curves for each topic, we employed two approaches to summarize the terms into topic from birth to adolescence: (1) averaging the correlation scores across team within the same topic at each time window (as shown in Fig 4), and (2) fitting the correlation scores using Generalized Additive Models (GAM). As shown in **Fig. S5-1,** solid lines represent the GAM-fitted curves based on the correlations of all contributing terms while dashed lines are correlations of individual terms for each topic.

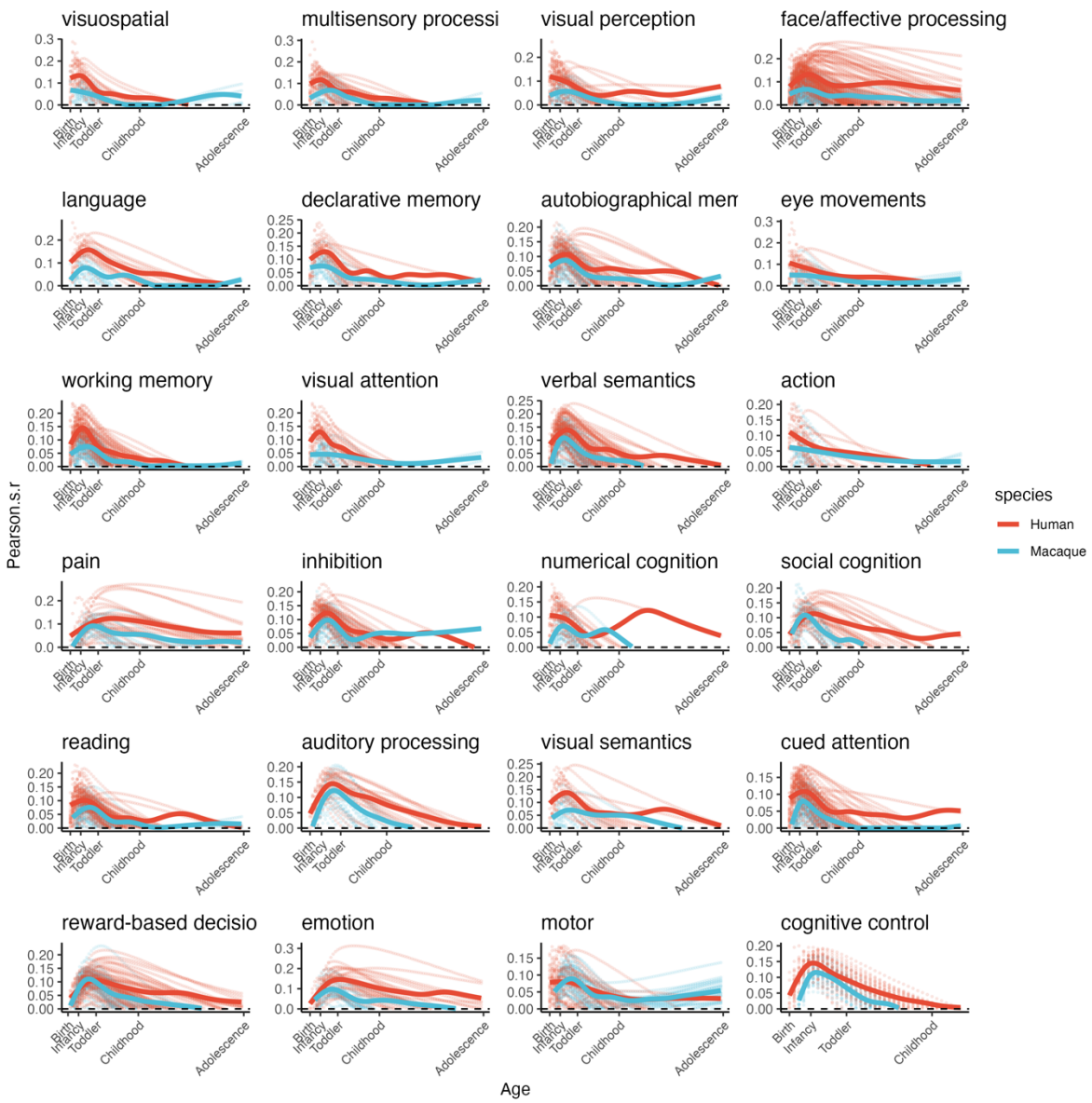

Fig. S5-1 | Decoded cognitive development trajectories from birth to adolescence for human (0-18 years) and macaque (0-6 years). Regional growth maps of gray matter volume with a progressively increased interval (human: per 3 months; macaque: per month) were decoded into cognitive terms using Neurosynth[15] meta-analysis. Dashed lines represent decoding correlation scores of individual terms. Solid lines represent the GAM-fitted curves from all contributing terms.

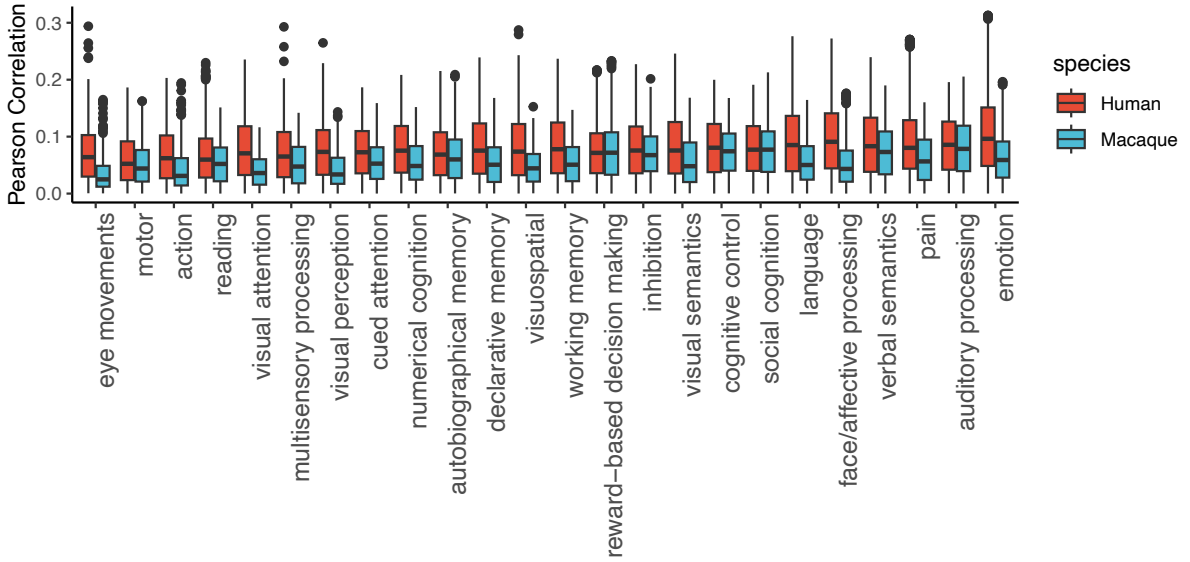

Fig. S5-2 | Distribution of decoded correlation scores from neurosynth[15] database for human and macaque. Each box shows the spread of correlations across developmental stages from birth to adolescence for all contributing terms within each topic.

6. Dataset Descriptions

Site-amu

The Aix-Marseille Université (AMU) dataset contains structural data from 4 rhesus macaques, 3 males and 1 female, ranging from 7 - 8 years of age. Animals were housed at the Institut de Neurosciences de La Timone. Animals were anesthetized with Isoflurane, and a Kopf frame and ear bars were used to hold the head for scanning. Monkeys entered the scanner in a sphinx position with a fiducial marker placed on the right side of the head. Heart rate and respiration were monitored during scanning.

Structural data was acquired with a Siemens Prisma 3T scanner, with a T1w voxel resolution of 0.8mm (TE: 2.04ms, TR: 2900 ms, TI: 1000ms), and a T2w voxel resolution of 0.8mm (TE: 561ms, TR: 3200 ms).

Site-amu-2

The second Aix-Marseille Universite (AMU) dataset[17] contains structural data from 20 rhesus macaques with 21 unique scans (6 male and 14 female). All experimental procedures were in compliance with the National Institutes of Health's Guide for the Care and Use of Laboratory Animals and approved by the Ethical board of Institut de Neurosciences de la Timone and authorized by the French Ministry of Higher Education, Research and Innovation.

The animals were housed in groups of 2 in enriched cages in a temperature and hygrometer-controlled room with a 12:12h light-dark cycle. A laboratory diet was provided twice daily, supplemented with fresh fruit and vegetables and *ad libitum* access to water. All procedures were performed under veterinary supervision with the objective to limit pain and discomfort and to promote animal welfare.

NHPs were first sedated by intramuscular injection of ketamine (10 mg/kg), midazolam (0.1 mg/kg), and glycopyrrolate (0.005 mg/kg). After the trachea was intubated and the lungs ventilated mechanically (ventilator Zeus, Drager, Lûbeck, Germany) with 2.3 vol% end-tidal sevoflurane (Baxter, Guyancourt, France) in a gas mixture of 40% oxygen and 60% nitrogen (figure 1A), a tidal volume of 6 mL/kg, and a PEP = 3 cmH_2O. Ventilation was adjusted to maintain an exhaled CO_2 level between 30 to 40 mmHg. NHPs were warmed by a heated blanket (Bair Hugger®, 3M, Minnesota, USA) to maintain a body temperature of 38.0±0.5°C throughout the procedure. Anesthesia was induced right before scanning and maintain throughout the MRI acquisition. During scanning, the animals were supine and anesthetized with foam in the MRI head coil. The MRI was performed on a Siemens 3T Prisma MRI scanner (Siemens Medical Solutions, Saint-Denis, France) and with different coils. More details on subject scanning acquisition parameters are specified below.

Scanning procedures involved collecting using a Scanmed (16CH pediatric coil) or a Siemens (Loop 11cm coil, 20CH Head-Neck coil, 24 CH macaque coil, or a 64CH Head-Neck coil) scanner. T1w images were collected using a selection of 6 sequences for different subjects, including: (1) T1w at 0.4mm isotropic with a slice thickness of 0.4mm, TR/TE/TI= 3300/3.13/1130ms, bandwidth (BW) of 210 Hz/pix, FOV of 128mm×128mm, flip angle of 8 degrees, matrix size of 320×320, GRAPPA=2, and 3 averages; (2) T1w at 0.7mm isotropic (sub-16) with a slice thickness of 0.7mm, TR/TE/TI= 2300/2.82ms, BW=210 Hz/pix, FOV of 180mm×151mm, flip angle of 8 degrees, matrix size of 256×216; (3) T1w at 0.8mm isotropic (MPRAGE sequence) with TR/TE/TI= 2300/4.05/912ms, flip angle of 8 degrees, BW=200 Hz/pix, FOV of 128mm×128mm, slice thickness of 0.8mm, matrix size of 160×160, and GRAPPA=2; (4) T1w at 0.6mm isotropic (MP2RAGE sequence) with TR/TE/TI1/TI2= 5000/2.91/700/2500ms, flip angles of 4/5 degrees, BW=270 Hz/pix, FOV of 135×126.6mm, slice thickness of 0.6mm, matrix size of 224×210, and 2 averages; (5) T1w at 0.5mm isotropic (MPRAGE sequence) with TR/TE/TI= 2800/4.24/1100ms, flip angle of 8 degrees, BW=210 Hz/pix, FOV of 128×128mm, slice thickness of 0.5mm, matrix size of 256×256, repeated 3 times separately; (6) T1w at 0.4mm isotropic (MPRAGE sequence) with TR/TE/TI= 2800/2.39/1150ms, flip angle of 8 degrees, BW=270 Hz/pix, FOV of 128×120mm, slice thickness of 0.5mm, matrix size of 320×300, repeated 3 times separately.

Site-ecnu

The East China Normal University (ECNU) dataset[18,19] includes anatomical data from 4 male rhesus macaques ranging from 32-45 months of age. Animals were housed at the University, either singly or in pairs, with automatically regulated lighting, and monkey chow and fruit provided twice a day. Water was available *ad libitum*. Monkeys were trained to watch videos and respond on touch screen apparatus. For scanning, monkeys were first anesthetized with atropine via injection, followed by Zoletil. Monkeys were then head fixed in a Stereotaxic frame with ear bars in a sphinx position in the MRI. During scanning, subjects were monitored with ECG and for respiration.

Structural scans were acquired with a Siemens 3T horizontal bore scanner and a surface coil. T1w data was acquired at a voxel resolution of 0.75 x 0.75 x 0.8mm (TE: 77 ms, TR: 3000ms) at a flip angle of 15 degrees. T2w data was acquired at a voxel resolution of 0.5 x 0.5 x 1.0mm (TE: 3.38 ms, TR: 2200 ms) at a flip angle of 120 degrees.

Site-ecnu-chen

The dataset from East China Normal University (Chen) contains T1w images from 10 male rhesus macaques. Monkeys were housed singly, with automatically regulated lighting; monkey chow and fruit given twice a day (280g in total) and water given twice a day (1000ml in total). For anesthesia, Atropine was applied via subcutaneous injection 20 min before anesthesia (dosage = body weight * 0.05mg/kg). Ketamine was used via subcutaneous injection (dosage = body weight * 0.15mg/kg). After, the monkeys were head-fixed on the Stereotaxic, Zoletil 50# was injected (dosage = body weight * 0.05ml/kg). Monkeys were scanned in the sphinx position in MRI stereotaxic apparatus.

T1w images were acquired with a 3T Siemens Trio with a surface coil. T1w data was acquired at a voxel resolution of 0.6mm isotropic and 0.75 x 0.75 x 0.8mm (TE: 2.69-3.71ms, TR: 2200 ms) and a flip angle of 7 and 9 degrees.

Site-emory

The Emory University longitudinal dataset[20–25] comprises 40 unique infant and juvenile rhesus macaques (23 males, 17 females), with a total of 83 scans. Age distribution ranges from 0.21 to 1.5 years, where most animals were scanned longitudinally at 2 weeks and 3, 6, 12 and 18 months of age. Animals were housed in big social groups in outdoor compounds with access to climate-controlled indoor areas. Standard, high fiber, and low-fat monkey chow diet (Purina Mills Int., Lab Diets, St. Louis, MO), seasonal fruits and vegetables were provided twice daily, in addition to enrichment items. Water was available ad libitum. All procedures were in accordance with the Animal Welfare Act and the U.S. Department of Health and Human Services “Guide for the Care and Use of Laboratory Animals” and approved by the Emory Institutional Animal Care and Use Committee (IACUC).

All monkeys were scanned at the Emory National Primate Research Center (ENPRC) Imaging Center, Emory University, and data were acquired with a Siemens 3T Trio scanner and an 8-channel surface coil. T1w data was acquired at a voxel resolution of 0.5mm3, isotropic (TR: 3000ms, TE: 3.51ms, TI: 950 ms) and a flip angle of 8 degrees. T2w data was acquired at 0.5x0.5x1mm3 voxel resolution (TR: 7900ms, TE: 125ms) and a flip angle of 90 degrees. Animals were scanned supine and the head immobilized in a custom-made head holder with ear bars and a mouthpiece to minimize motion. Following initial induction of light anesthesia with telazol and endotracheal intubation, MRI scans were collected under isoflurane anesthesia (0.8-1%, inhalation) following published approaches for studies of macaque neurodevelopment (Kovacs-Balint et al., 2021; Mavigner et al., 2018; Raper et al, 2020; Shi et al, 2017). Physiological parameters were monitored using an oximeter, ECG, rectal thermistor, and blood pressure monitor. An intravenous catheter was used to administer dextrose/NaCl for hydration, and the animal was placed over an MRI-compatible heating pad to maintain temperature.

Site-ion

The Institute of Neuroscience (ION) dataset[26] contains data from 8 rhesus macaques, 7 male and 1 female, with an age distribution of 3.8 - 6 years. Animals were housed at the Institute of Neuroscience, Shanghai, in single cages. Anesthesia of the animals was inducted with an intramuscular injection of a cocktail of dexmedetomidine (18 - 30 μg/kg) and midazolam (0.2 - 0.3 mg/kg), supplemented with atropine sulfate (0.05 mg/kg). After intubation, anesthesia was maintained using the lowest possible concentration of isoflurane gas via a MRI-

compatible ventilator. Monkeys were fixed in the sphinx position for scanning with a custom-built MRI-compatible stereotaxic frame. Physiological parameters including blood oxygenation, ECG, rectal temperature, respiration rate and end-tidal CO2 were monitored. Oxygen saturation was kept over 95%. Animals were ventilated by an MRI-compatible ventilator. Body temperature was kept constant using a hot water blanket.

Data was acquired with a Siemens Tim Trio 3T whole-body scanner and an 8-channel phased-array transceiver coil. Structural MRI data was acquired for T1w with an MPRAGE sequence, at a voxel resolution of 0.5mm (TE: 3.12 ms, TR: 2500ms, TI: 1100ms) and a flip angle of 9 degrees.

Site-kmust

The rhesus macaques were randomly selected from a large monkey group housed at the State Key Laboratory of Primate Biomedical Research, Institute of Primate Translational Medicine, Kunming University of Science and Technology for MRI scanning. Thirty-one macaques were included in the current study (8 males and 23 females, age range = 10-20 years). All the experimental procedures were in accordance with the guidelines for the National Care and Use of Animals and the experimental protocols and were approved by the National Animal Research Authority of China and the Institutional Animal Care and Committee of the State Key Laboratory of Primate Biomedical Research, Institute of Primate Translational Medicine, Kunming University of Science and Technology.

The MRI data were acquired using Siemens 3T Prisma scanner. Before scanning, the monkeys were untrained and pre-anesthetized with Sumianxin (0.1 ml/kg), Zolatil (0.1 ml/kg) and atropine (0.1 ml/kg). After the anesthesia is stable, the MRI scanning of T1-weighted images were acquired using the following parameters: TR/TE = 1400/3.55 ms, FA = 8°, in-plane acquisition matrix = 224 × 224, at a voxel resolution of 0.6 mm isotropic.

Site-lyon

The dataset from the Lyon Neuroscience Research Center includes scans from female 4 rhesus macaques with an age range of 5 - 12 years. The project was authorized by the French Ministry for Higher Education and Research (project no. 20-12-0401-005) in accordance with the French transposition texts of Directive 2010/63/UE, based on ethical evaluation by the French Committee on the Ethics of Experiments in Animals (C2EA) CELYNE registered at the national level as C2EA number 42. T1w data was acquired with a Siemens Sonata 1.5T and a Siemens Prisma 3T scanner. T1w data was collected with an isotropic resolution of 0.6mm (TE: 2.89ms, TR: 2.16s, TI: 1.1s) with a flip angle of 15 degrees.

Site-mcgill

McGill University's McConnell Brain Imaging Centre dataset includes 1 rhesus macaque (female), aged 12 years. Animals were housed in pairs, and animal care protocols followed the Animal Care Committees of the Montreal Neurological Institute and McGill University. For scanning, the animal was intubated and anesthetized with 0.6%-1.2% isoflurane. The animal was scanned 30 minutes after intubation. Anesthesia was maintained throughout the MRI session and scanned in the supine position. Heart beat and oxygen saturation were monitored by means of pulse oximetry. The macaque was ventilated, and core temperature was monitored and maintained at 38 degrees by means of a heating pad.

T1w and T2w data was acquired with a Siemens 3T Trio scanner, and a custom-made 8-channel phased-array receive head coil. T1w data was acquired with a MP2RAGE sequence with a voxel resolution of 0.6mm isotropic (TE: 3.65 ms, TR: 5000 ms, TI: 700 ms) and a flip angle of 4 degrees. T2w data was acquired with a T2 SPACE sequence, at a voxel resolution of 0.6mm isotropic (TE: 320 ms, TR: 3200 ms) and a flip angle of 120 degrees.

Site-mountsinai-P

Site-mountsinai-P contains data[27] of 8 male rhesus macaques with an age distribution of 3.4 - 8 years. Monkeys were housed at the Icahn School of Medicine at Mount Sinai (ISMMS). Monkeys were housed in groups, indoors, in standard primate caging. All monkeys received environmental enrichment consisting of toys and novel food items. All monkeys received cognitive tests in touch screen apparatus. For scanning, monkeys were anesthetized with ketamine and buprenorphine prior to intubation and placement in a stereotaxic frame, where they entered the MRI in a sphinx position feet first. Monkeys were physiologically monitored throughout scanning to ensure body temperatures, pulse rates, blood pressure, etc.

All imaging data was acquired with a Philips Achieva 3T scanner, and a 4-channel phased array coil. Anatomical T1w scans were acquired at a voxel resolution of 0.5mm (TE: 6.93ms, TR: 1500ms, TI: 1100ms), with a flip angle of 8 degrees. T2w scans were also acquired at 0.5mm voxel resolution (TE: 366ms, TR: 2500ms).

Site-mountsinai-S

The Mount Sinai School of Medicine (Siemens) contains MRI data of 6 adult male rhesus macaques, aged from 5.3-6.3 years. All animals were housed at the Icahn School of Medicine at Mount Sinai. Monkeys were housed in groups of 6 indoors in standard primate caging, in housing rooms containing other monkeys. All monkeys received environmental enrichment consisting of toys and novel food items, in addition to cognitive tests via touch screen apparatus. For scanning, animals were anesthetized with ketamine, meloxicam, and buprenorphine prior to intubation and placement in a stereotaxic frame. Monkeys were scanned in the sphinx position, head first.

Structural data was acquired with a Siemens Skyra 3T scanner and a 4-channel clamshell coil. T1w data was acquired at a voxel resolution of 0.5mm (TE: 3.02ms, TR: 2700 ms, TI: 800ms). T2w scans were also acquired at a resolution of 0.5mm (TE:539ms, TR: 3200 ms).

Site-neurodev

The longitudinal dataset[28] includes 33 macaques (*macaca mulatta*) with a total of 160 scans. The dataset includes 18 males and 15 females, with an age range of 0.003 and 3 years. Housing consisted of stainless steel caging (each 0.9 x 0.9 x 0.9 m), where each female monkey lived with her infant, either individually or as a pair with another adult female in double cages. Animals were fed a standardized diet of commercial biscuits and fruit supplements and foraging devices for enrichment. Water was available *ad libitum,* the temperature was controlled at 21.5 degrees celsius, and the light/dark cycle was maintained at 14:10 with lights on at 06:00. All infants were reared normally by their mothers until weaning occurred at 6-7 months of age. Afterwards, the older juveniles were housed in small social groups or as a pair to provide companionship. The research protocol was approved by the Institutional Animal Care and Use Committee (IACUC). Care and treatment of the animals at HPL are designed to meet and exceed the guidelines promulgated by the National Institutes of Health Guide for

the Care and Use of Laboratory Animals. The quality of the research findings is predicated on the high quality of care.

Subjects were given a pre-anesthetic (ketamine hydrochloride 10 mg/kg I.M.) for transport to the MRI facility. For infants younger than 6 months of age, immobilization during the scan was achieved with inhalant isoflurane (1.5%). Older subjects were immobilized throughout the scanning procedure by an initial administration of ketamine hydrochloride (10 mg/kg I.M.) followed by dexdomitor (0.015 mg/kg I.M.). The effects were reversed at the end of the session by administering atipamezole (0.15 mg/kg I.V.). The plane of anesthesia was monitored with a pulse oximeter to track heart rate and oxygen saturation in both younger and older subjects.

Scans were performed on a GE MR750 3.0T scanner (General Electric Medical, Milwaukee WI) using the human 8-channel brain array coil at the Waisman Laboratory for Brain Imaging and Behavior at the University of Wisconsin-Madison. In order to ensure a safe plane of anesthesia and recovery, the scanning protocol for animals younger than 6 months lasted approximately 30 min. For subjects older than 6 months of age, the scanning procedure was extended to slightly <1 h to improve the signal-to-noise ratio on the diffusion weighted image (DWI) scan.

High-resolution 3D T1-weighted imaging was performed using an axial Inversion Recovery (IR) prepared fast gradient echo (fGRE) sequence (GE BRAVO) (*TI* = 450 ms, *TR* = 8.684 ms, *TE* = 3.652 ms, FOV = 140 × 140 mm, flip angle = 12°, matrix = 256 × 256, thickness = 0.8 mm, gap = −0.4 mm, 80 percent field-of-view in phase encoding direction, bandwidth = 31.25 kHz, 2 averages, total time = 10:46 min) provided an effective voxel resolution of 0.55 × 0.55 × 0.8 mm across the entire cranium. The T2-weighted scan was performed using a sagittal 3D CUBE FSE sequence (*TR* = 2500 ms, *TE* = 87 ms, FOV = 154 × 154 mm, flip angle = 90°, matrix = 256 × 256, 90 percent field of view in the phase encoding direction, slice thickness = 0.6 mm, gap = 0 mm, bandwidth = 62.5 kHz, ARC parallel imaging with a factor of 2 acceleration in both phase encoding and slice encoding directions, total time = 6:36 min) across the cranium was acquired with a voxel resolution of 0.6 × 0.6 × 0.6 mm.

Site-newcastle

Newcastle University provided a dataset[29–35] of 14 macaques (12 male, 2 female), aged 3.9 to 13.14 years. All animals were housed and cared for in a group-housed colony, and animals performed behavioral training on various tasks for auditory and visual neuroscience. Animals head fixation included an MRI compatible head-post or non-invasive head immobilization, scanned upright and working on tasks or at rest. All animals had eye tracking, video, and audio monitoring during the procedure. All but two animals were scanned awake.

All scans were performed using a Vertical Bruker 4.7T scanner specifically designed for primates, with either a single-channel or a 4-8 channel parallel imaging coil. For each subject's session, the MDEFT sequence was used. The anatomical (T1) images were captured using a magnetization-prepared rapid gradient echo (MPRAGE) technique. Each subject had one scan with no acceleration applied. The settings included a flip angle of 90 degrees, an echo time (TE) of 3.74 ms, a repetition time (TR) of 2000 ms, and a bandwidth of 284.

Site-NIMH

The NIMH dataset[36–38] includes T1 and T2 data from 3 rhesus macaques, with an age distribution of 5-7 years (2 female, 1 male). All procedures were approved by the Animal Care and Use Committee of the US National Institutes of Health (National Institute of Mental Health) and followed US National Institutes of Health guidelines. The animals were on water restriction and received their daily fluid intake during their daily testing. Each subject's weight and hydration level was monitored closely and maintained throughout the experimental testing phases. Animals were pair-housed throughout the length of the study. Animals were implanted with a custom-designed and fabricated fiberglass head-post, which was used to immobilize the head during testing. During testing, animals eye movements were monitored.

MRI data was acquired with a Bruker BioSpec Vertical 4.7T scanner with a Bruker S380 gradient coil. T1 data was acquired at a voxel resolution of (1.5mm x 0.5mm x 0.5mm).

Site-NIMH-CT

The NIMH-CT dataset[39] includes 3 macaques (2 male, 1 female) with an age distribution of 3 - 6 years. Animals were housed according to the National Institutes of Health Guide for the Care and Use of Laboratory Animals, at the Central Animal Facility at the NIMH. Monkeys were trained to perform a fixation task, with a central fixation spot and complex visual objects. All subjects were anesthetized with isoflurane before anatomical scans. One eye was monitored visually and gaze direction was recorded for periods when the eye was open.

Anatomical scans for morphometric analysis and alignment of resting state data were collected on a horizontal 4.7T Bruker scanner. Anatomical scans for morphometric analysis and alignment of resting state data were collected with a single loop volume coil. T1w data was collected with an isotropic resolution of 0.6mm (TE: 2.89ms, TR: 2.16s, TI: 1.1s) with a flip angle of 15 degrees.

Site-nin

The Netherlands Institute for Neuroscience (NIN) dataset includes data for 2 rhesus macaques, both male. Data ranges from 5-6 years old. All experiments were approved by the Institutional Animal Care and Use Committee of the Royal Netherlands Academy of Arts and Sciences. The animals were implanted with custom-made PEI/PEEK head holders fixed to the skulls with ceramic screws (Thomas Recording) and acrylic cement (Palacos R+G). The macaques were sedated with Medetomidine 0.08 ml/kg (concentration 1 mg/ml) and Ketamine 0.07 ml/kg (concentration 100 mg/ml) is given intramuscularly. If the procedure is still ongoing after ~60 minutes, another dose of 0.07 ml/kg Ketamine is given.

Data was scanned with a Philips Ingenia 3T and an 8-channel phased array receive coil (KU Leuven). T1w's were acquired at 0.6mm voxel resolution (TE: 6ms, TR: 13ms, TI: 900ms) with a flip angle of 8 degrees.

Site-nki

The Nathan Kline Institute (NKI) dataset[40] includes data for 2 rhesus macaques, one male and one female. Data ranges from 6-7 years old. All methods and procedures were approved by the NKI Institutional Animal Care and Use Committee (IACUC) protocol. The monkeys were previously implanted with an MRI-compatible custom built acrylic head post. The macaques were sedated with an initial dose of atropine (0.05 mg/kg IM), dexdomitor (0.02 mg/kg IM) and

ketamine (8 mg/kg IM) intubated, and maintained with 0.75% isoflurane anesthesia for the duration of structural MRI procedures.

Data was scanned with a Siemens Tim Trio 3T and an 8-channel surface coil. T1w's were acquired at 0.5mm voxel resolution (TE: 3.87ms, TR: 2500ms, TI: 1200ms) with a flip angle of 8 degrees.

Site-NKIdev

The Nathan Kline Institute (NKI) development dataset collected longitudinal MRI data from 3 animals including 83 scans in total. Dataset comprises of 1 male and 2 females, scanning from around birth to 1.5 years of age. Data was scanned with a Siemens Tim Trio 3T and a 32 channel siemen's coil. T1w data was acquired with a voxel resolution of 0.7mm.
The macaques were sedated with an initial dose of dexdomitor (0.01-0.015 mg/kg IM) and ketamine (5 mg/kg IM). An IV was placed and a saline drip that administered 0.001 mg/kg/hr of dexdomitor to help maintain anesthesia levels. In addition, the animals were masked and maintained with 0.75-1.0% isoflurane for the duration of the MRI procedures.

Site-ohsu

The dataset from Oregon Health and Science University contains 2 rhesus macaques (both male) aged 5 years. Animals were indoor housed with pre-established male partners of similar age. Pairs were separated for fasting the night before a scan and reunited once fully awake post scan. Animal husbandry and care is maintained by ONPRC Department of Comparative Medicine clinical and behavioral support was provided by the Clinical Services Unit and the Behavioral Services Unit respectively. The animal procedures were conducted in accordance with National Institutes of Health guidelines on the ethical use of animals and were approved by the Oregon National Primate Research Center (ONPRC) Institutional Animal Care and Use Committee. After an overnight fast, the animals were sedated by IM injection with 10 mg/kg of ketamine for removal from cage and transport, intubation and catheter placement. Once intubated the sedation level was maintained with 1-1.5% isoflurane. At this time 8-12 mls of blood was drawn from the femoral vein for blood iron level monitoring and blood banking. Rectal temperature was taken pre and post scan. Time between initial ketamine sedation and placement in the coil averaged 20 mins.

During scanning, the head was supported in coil with the use of foam padding and wedges. Animals were continuously monitored remotely for SpO2, respiratory rate, ETCO2, pulse and blood pressure throughout the scan with measurements being recorded every 10-15 mins. Body temperature was maintained with a recirculating water mat and room temperature regulation. Catheter was kept patent with the remote administration of 0.5-1 mL of saline solution IV at regular intervals.

All scans were collected using a 3 Tesla Siemens Tim Trio scanner with a 15-channel knee coil. Optimization of the magnetic field was performed prior to data acquisition. T1w data was acquired with a MPRAGE sequence at a voxel resolution of 0.5 × 0.5 × 0.5 mm (TE: 3.33ms, TR: 2600ms, TI: 900ms) with a flip angle of 8°. T2w data was acquired at a voxel resolution of 0.5 × 0.5 × 0.5 mm (TE: 407 ms, TR: 3200 ms).

Site-OHSU-CU

This dataset came from a study that was approved by the Institutional Animal Care and Use Committee (IACUC) of the Oregon National Primate Research Center (ONPRC)[41] and met all federal regulatory requirements set forth in the *Guide for the Care and Use of Laboratory Animals*. The dataset includes 24 macaques with 24 scans, consisting of 12 males and 12 females scanned across an age range of 1 to 2.92 years. The NHPs were first sedated with ketamine 5 mg kg^{-1} i.m. and subsequently anesthetized with 3% isoflurane with tracheal intubation. The NHPs were then placed on a mechanical ventilator and isoflurane reduced to 1%. This concentration of isoflurane, which was maintained for the entire duration of the MRI (30–45 min). The NHPs were monitored, and their physiological parameters controlled throughout anesthesia. were placed headfirst and supine into a Siemens 3T Tim Trio (Erlangen, Germany) paired with a quadrature transmit, 15-channel receive human “extremity” RF coil (QED, Cleveland, OH). Data acquisition included four T1-weighted structural images (repetition time [TR]=2500 ms, time echo [TE]=3.86 ms; 0.5 mm iso-voxels, 128 slices, field of view [FOV]=108×128 mm).

Site-OHSU-fetal

The dataset from the Oregon National Primate Research Center[1] contains brain volumes derived from T2 weighted Half-fourier Acquisition Single-shot Turbo spin-Echo (HASTE) acquisitions of 28 pregnant macaques consisting of 43 total scans. Subjects ranged from gestational day (G)85 to G135 (before birth) at time of scanning. The dataset consists of 13 male and 15 female fetuses. Experimental procedures were approved by the Oregon National Primate Research Center (ONPRC) Institutional Animal Care and Utilization Committee (IACUC) and conformed to the guidelines set by the National Institute of Health (NIH). Dams were socially housed indoors and given chow rations twice daily and ad libitum access to water. Light cycle was set at 12 hrs light/dark. For scanning, dams were first sedated with 5-15 mg/kg ketamine IM, followed by intubation and maintenance of anesthesia with 1-2% isoflurane vaporized in 100% oxygen. Dams were placed headfirst and supine into a Siemens 3T Tim Trio (Erlangen, Germany) paired with a quadrature transmit, 15-channel receive human “extremity” RF coil (QED, Cleveland, OH). Physiological parameters including pulse rate, arterial oxygen saturation, and respiration were monitored through scanning procedures.

Site-OHSU-UIUC

Site-OHSU-UIUC, provided from Oregon Health and Science University[42], comprises 22 (10 males, 12 females) macaques with 65 scans, ranging from 0.16 to 0.5 years of age. Data was acquired with a 3T Siemens Tim Trio and a 15 channel knee coil. T1w data was acquired with an MPRAGE sequence at a voxel resolution of 0.5mm (TE: 3.33ms, TR: 2600ms, TI: 900ms) and a flip angle of 8 degrees. T2w data was acquired at a voxel resolution of 0.5mm (TE: 407 ms, TR: 3200 ms).

Animals were born and housed at the Oregon National Primate Research Center. They received from birth either 1) a combination of breastmilk, a standard nonhuman primate laboratory diet (Monkey Diet Jumbo 5037, Lab Diet, St. Louis, MO, USA) and a variety of fruits and vegetables, or 2) one of two nutritionally adequate infant formulas differing in carotenoid content (Liu et al., 2018; Miranda-Dominguez et al, 2022).

For scanning, monkeys were sedated with an initial dose of ketamine (5 mg/kg), intubated,

and maintained at ~1% isoflurane anesthesia; respiratory rate, pulse rate, end tidal CO2, and oxygen saturation were monitored every 10 minutes throughout the procedure.

Site-oxford

The Oxford dataset[43–45] contains structural MRI data from 20 male rhesus macaques ranging from 2.41 - 6.72 years of age. Monkeys were housed in groups at the Wellcome Centre for Integrative Neuroimaging. Data was acquired with a 3T whole body scanner and a four-channel, phased-array, radio-frequency coil in conjunction with a local transmission coil. Due to an agreement between the initial data collectors and the scanner manufacturer, they did not disclose the scanner manufacturer. Monkeys were anesthetized during scanning with ketamine (10 mg/kg) combined with either xylazine (0.125-0.25mg/kg) or midazolam (0.1mg/kg) and buprenorphine (0.01mg/kg). Macaques also received injections of atropine (0.05 mg/kg, i.m.), meloxicam (0.2 mg/kg, i.v.), and ranitidine (0.05 mg/kg, i.v.). Local anesthetic (5% lidocaine/prilocaine cream and 2.5% bupivacaine injected subcutaneously around the ears to block peripheral nerve stimulation) was also used at least 15 min before placing the macaque in the stereotaxic frame. Anesthesia was maintained with isoflurane. Scanning commenced 1.5-2 hours after induction, when the peak effect of ketamine was unlikely to still be present. Animals were placed in an MRI-compatible stereotactic frame in a sphinx position for data acquisition. Structural data was acquired with an MPRAGE sequence at a voxel resolution of 0.5mm (TE: 4.01ms, TR: 2500ms, TI: 1100ms) with a flip angle of 8 degrees.

Site-princeton

The Princeton University Animal Care and Use Committee approved all procedures, which conformed to the National Institutes of Health guidelines for the humane care and use of laboratory animals.

Two male rhesus macaques (Macaca mulatta, ages = 3 years, body weights = 4.7/5.5kg) were scanned on a Siemens MAGNETOM Prisma 3T using an 11cm loop coil (Siemens, Erlangen, Germany). For all scan sessions, animals were first sedated with ketamine (10 mg/kg IM) and maintained with isoflurane gas (2.5–3.0%) using an MR-compatible anesthesia workstation (Integra SP II, DRE Inc, Louisville KY). Animals were placed in the "sphinx" position and their heads fixed using an MR-compatible stereotaxic frame (1430M, David Kopf Instruments, Tujunga CA). Siemens wireless physiology sensors were used to monitor EKG, pulse, and respiratory rate. Body temperature was monitored using a fiber optic probe (FOTS100, BioPac Systems Inc, Goleta CA). Blood oxygen (SpO2) and end-tidal carbon dioxide (ETCO2) were monitored with an MR-compatible patient monitor (Model 3150, InVivo Corp, Pleasanton CA). Artificial ventilation was used to maintain normocapnia. Normothermia was maintained using blankets and a warm water recirculating pump (Gaymar STP700 T/Pump, Stryker Corp, Kalamazoo MI) modified with long tubing to reach the MRI bore.

Three T1-weighted volumes were collected with an 3D MPRAGE sequence at a 0.5mm voxel resolution (TR=2700 ms, TE=2.32ms, TI=850 ms, flip angle=9 deg, averages=3). One T2-weighted volume was collected at the same resolution with a 3D SPACE sequence (TR=3500ms, TE=398ms, averages=1).

Site-queens

The dataset from Queens University includes 13 scans from 13 cynomolgus macaques (*Macaca fascicularis*, 6-11 yrs, mean=7.5yrs; body weight: 6.3-12.8 kg). All non-human primates were housed at the Centre for Neuroscience Studies at Queen's University (Kingston, Ontario, Canada) under the care of a lab animal technician and the Institute Veterinarian. All procedures were approved by the Queen's University Animal Care Committee and were in full compliance with the Canadian Council on Animal Care. The neuroimaging data was acquired using a 3T MRI scanner (MAGNETOM Prisma, Siemens, Erlangen, Germany) and a 24-channel macaque head coil designed by the Robarts Research Institute for use in the 3T environment (University of Western Ontario).

During scanning, anesthesia was induced with ketamine (6 mg/kg, intramuscular) and dexmedetomidine (4.5 ug/kg, intramuscular). Glycopyrrolate (0.013 mg/kg, intramuscular) was given and the animal was intubated (4.0 endotracheal tube) and placed on isoflurane anesthesia (0.5-1%). A catheter was inserted into the saphenous vein, and after the animal was transferred into the MRI bore, anesthesia was maintained using intravenous dexmedetomidine (DEX) (4.5 µg/kg/hr) and 0.6% isoflurane via a calibrated vaporizer with 100% oxygen at 1.5l/min. The anesthesia protocol was based on literature on relative preservation of functional connectivity in DEX anesthesia in macaques (Autio et al., 2020). Body temperature was maintained with an MRI-safe ConRad Thermal Blanket (DRE Veterinary). SPO2, heart rate, EKG, respiration rate and non-invasive blood pressure.

T1w data was collected with an isotropic resolution of 0.5mm (TE: 2.23ms, TR: 2.2s, TI: 0.9s) with a flip angle of 8 degrees. T2w data was also collected with an isotropic resolution of 0.5mm (TE: 0.562s, TR: 3.2s) and a flip angle of 120 degrees.

Site-rockefeller

The Rockefeller University dataset[46] includes anatomical data from 6 monkeys. The species included were 5 Macaca mulatta and 1 Macaca fascicularis, with an age distribution of 3-5 years and weight distribution between 5.4-7.3 kg. All animals were male. The animals were pair-housed, with all animal procedures conducted following the National Institutes of Health Guide for Care and Use of Laboratory Animals, and were approved by the Institutional Animal Care and Use Committees of The Rockefeller University (protocol number 12585-H) and Weill-Cornell Medical College (protocol number 2010–0029).

Monkeys were induced with ketamine (3 mg/kg) and dexmedetomidine hydrochloride (0.02 mg/kg), and anesthesia was maintained with isoflurane (0.5%-0.6%). The time between anesthesia and scanning was minimal, with monkeys placed in the scanner as soon as isoflurane anesthesia was stable. Head fixation was achieved with a head-post attached to an acrylic headcap, and monkeys were scanned in the sphinx position. An IV contrast agent, ferumoxytol (8–10 mg per kg of body weight), was administered. During scanning, physiological monitoring included electrocardiogram (sampling rate 400 Hz) and breathing rate (sampling rate 50 Hz).

All scans were collected using a Siemens TIM Trio 3T scanner with AC88 gradient. An 8-channel phased-array receive coil with a single loop transmit coil was used. Structural T1: MPRAGE sequence was used, with a voxel resolution of 0.5 × 0.5 × 0.5 mm, TE: 2.95ms, TR: 2300ms, TI: 1100ms, and a flip angle of 8°.

Site-sbri

The Stem Cell and Brain Research Institute (SBRI) provided a dataset[47–55] of 16 rhesus macaques, 9 male and 7 female, with an age distribution of 3.6 - 13.7 years. Animals were all housed at the Stem Cell and Brain Research Institute in groups. For structural acquisition, monkeys were anesthetized with 15mg/kg of Zoletil 30 minutes after premedication with 0.1 mg/kg atropine sulfate. A MRI-compatible stereotaxic frame (Kopf, CA, USA) was used to secure the head and reduce variability in the measure. Scans were acquired with the monkey in a sphinx position, head first into the scanner. During all procedures heart rate and PO2 were monitored. During isoflurane anesthesia, ventilation parameters and C02 were also monitored. Data were sampled at 1/15min for vet record. None of these parameters were recorded continuously. The animal was intubated and ventilated with oxygen enriched air and 1% Isoflurane. Data was acquired with a Siemens 1.5T scanner, with a T1w voxel resolution of 0.6mm (TR: 2.16s, TE: 2.89s).

Site-ucdavis

In the first data release, site-ucdavis (University of California, Davis, Center for Neuroscience and California National Primate Research Center, Davis) provided anatomical data from 19 female rhesus macaques, ranging from 18.5-22.5 years of age. The California National Primate Research Center (CNPRC) is staffed with 7 full-time veterinarians and an extensive staff of veterinary and husbandry technicians. Monkeys were housed in pairs (N=16) or singly (N=4) indoors in standard primate caging, in housing rooms containing other rhesus monkeys. Single-housed monkeys had failed repeated attempts to find compatible cage mates from elsewhere in the colony. All monkeys received environmental enrichment consisting of toys and novel food items. Monkeys were anesthetized with ketamine, dexmedetomidine, and buprenorphine prior to intubation and placement in stereotaxic frame, with isoflurane maintenance anesthesia. Monkeys were scanned in the sphinx position, head first. During scanning, monkeys had the following measurements monitored: pulse rate, SpO2, end tidal CO2, inspired/expired isoflurane, blood pressure.

Structural data was acquired with a Siemens Skyra 3T and a 4-channel clamshell coil. T1w data was collected with a voxel resolution of 0.3mm (TE: 3.65ms, TR: 2500ms, TI: 1100ms), and a flip angle of 7 degrees. T2w data was also collected with a voxel resolution of 0.3mm (TE: 307ms, TR: 3000ms).

Site-ucdavis-2

The second release of data from the University of California, Davis[56–60] is comprised of two longitudinal datasets, with 388 structural scans from 56 unique macaques. The dataset includes 28 females and 28 males, with an age range of 0.02 - 11.48 years. Data was acquired with two different MRI scanners; a 3T Siemens Trio scanner (T1w sagittal data was collected with a voxel resolution of 0.7mm isotropic (TE: 4.73ms, TR: 2.2s, TI: 1.1s with a flip angle of 7 degrees.) and a 1.5T GE Genesis Signa (TE:6ms, TR: 27ms, flip angle 30, voxel size 0.625 x 0.625 x 0.7 mm). T2w data was also collected with a voxel resolution of 0.3mm and a flip angle of 5 degrees. Propofol was the anesthetic used at both scanners and was delivered with an MRI compatible IV pump.

Site-ucdavis-3

The third release of data from the University of California, Davis[61] includes 95 scans from 95 rhesus macaques, with 44 males and 51 females, and an age range of 2 to 6 years. Subjects were selected from large social groups living in outdoor corrals, and were temporarily pair housed indoors during the week of scanning. All procedures were approved by and adhered to guidelines established by the Institutional Animal Care and Use Committee. Prior to scanning, the subjects were anesthetized with ketamine (~10 mg/kg body weight), intubated, and placed on isoflurane anesthesia. Anesthesia was maintained with 1-2% isoflurane gas throughout the scanning. Once fully anesthetized, the subjects were fixed within an MRI-compatible stereotaxic frame and placed inside the magnet in the sphinx position. Heart rate, respiration, and oxygen saturation were continuously monitored during the scan.

Structural data was acquired using a 3T Siemens Skyra scanner and a dedicated rhesus 8-channel surface coil. T1-weighted scans were collected at a voxel resolution of 0.3 mm isotropic (TE: 3.368 ms, TR: 2.5 s, TI: 1.1 s) with a flip angle of 7 degrees.

Site-uwmadison

The UW-Madison Rhesus MRI dataset[62–70] is one of the PRIME-DE datasets, including anatomical data from 592 macaque monkeys at two different sites. Subject ages range from 0.8-4.5 years, with 327 males and 265 females. Monkeys were housed at the Wisconsin National Primate Research Center and the Harlow Center for Biological Psychology. Standard husbandry in a temperature- and humidity-controlled vivarium included a 12-h light/dark cycle, daily feeding sessions, ad libitum access to water, and daily enrichment. For scanning, monkeys were anesthetized using ketamine (15mg/kg, IM), then given medetomidine (0.03 mg/kg, IM) or dexmedetomidine (0.015 mg/kg, IM). Additional doses of ketamine were administered as needed to maintain anesthesia. Head fixation for scanning included a custom MRI compatible stereotaxic frame, with ear and tooth bars that fit inside the MR coil. Monkeys were scanned in the sphinx position with the nose pointing into the scanner. Heart rate and oxygen saturation were monitored continuously and recorded at minimum every 15 minutes throughout the MR imaging procedure. Heated water bags, bottles, or pads and towels, blankets, and bubble wrap were used to maintain body temperature during imaging.

Scanning sequences at the Wisconsin National Primate Research Center included anatomical scans with a GE Discovery MR750 3T scanner. Voxel resolution is 0.2734 x 0.5 x 0.2734 mm (TE: 5.412ms, TR: 11.4ms, TI: 600ms), with a flip angle of 10 degrees and a slice gap of 0.5mm. Monkey MRI data at the Harlow Center for Biological Psychology was acquired with a GE Signa Excite 3T scanner, at a voxel resolution of 0.2734 x 0.5 x 0.2734 mm (TE: 1.88ms, TR: 8.648ms, TI: 600ms), with a flip angle of 10 degrees and a slice gap of 0.5mm.

Site-uminn

Ten rhesus macaque monkeys[71–75] (macaca mulatta) were scanned on a Siemens 7T with a 4-channel clamshell coil (Langore NMRBio_2020). All animal procedures were approved by the Institutional Animal Care and Use Committee of the University of Minnesota and complied with United States Public Health Service policy on the humane care and use of laboratory animals. Monkeys received ketamine 10 mg/kg, midazolam 0.25mg/kg, and atropine 0.04mg/kg IM and were intubated and maintained on isoflurane (1-3%, inhalation) during the scan. The animal was wrapped in warm packs to maintain body temperature. A circulating water bath was used to provide additional heat. A ventilator was used to prevent atelectasis

of the lungs, and to regulate CO2 levels. The animal was observed continuously, and vital signs and depth of anesthesia were monitored and recorded at 15-min intervals. Rectal temperature (99.6 F), respiration (10-15 breaths/min), end-tidal CO2 (25-40), electrocardiogram (70-150 bpm), and oxygen saturation (>90%) were monitored using an MRI compatible monitor (IRadimed 3880 MRI Monitor, Winter Springs, FL).

All animal procedures were approved by the Institutional Animal Care and Use Committee of the University of Minnesota and complied with United States Public Health Service policy on the humane care and use of laboratory animals.

For scanning, T1w data was acquired with an MPRAGE sequence at 0.5mm isotropic resolution (TR: 3500 ms, TE: 3.56 ms, FOV: 131 x 150). T2w data was acquired with a 2D Turbo spin echo sequence, at 0.58 mm isotropic resolution (TR: 8000 ms, TE: 68 ms, FOV: 112 x 150) with a flip angle of 120 degrees.

Site-uwo

The University of Western Ontario (UWO) dataset[76] includes T1w scans from 2 rhesus macaques, both male, ranging from 4 to 7 years of age. Experimental procedures on nonhuman primates were in accordance with the Canadian Council of Animal Care policy and a protocol approved by the Animal Use Subcommittee of the University of Western Ontario Council on Animal Care. Animals were housed in pairs. For scanning, animals were first sedated with 0.1-0.2 mg/kg acepromazine, followed by 7.5 mg/kg ketamine hydrochloride by intramuscular injection. Anesthetic induction was accomplished by the administration of 2.5mg/kg propofol via an intravenous catheter in the saphenous vein. Anesthesia was maintained with 1 to 2% isoflurane with oxygen (1.5-2 L/min) through endotracheal intubation and it was reduced to 1% during fMRI acquisition. Monkeys entered the scanner in the sphinx position. Heart rate and SpO2 were monitored throughout via a pulse oximeter and end-tidal CO2 and respiration rate were monitored via a capnometer. Temperature was recorded before and after the scans and was maintained within the normal range using heating discs, covers, and thermal insulation. Animals received subcutaneous fluids (10 ml/kg/hr) before and after the scan.

Structural scans were acquired with a Siemens Magnetom 7T scanner and a custom-made 24-channel phased array receive coil with an 8-channel transmit coil. An MPRAGE sequence was used for T1w, acquired at a voxel resolution of 0.5mm (TE: 3.88ms, TR: 6500ms, TI: 800ms) at a flip angle of 4 degrees.

Site-wake-forest

The dataset from the Wake Forest University School of Medicine[77] includes 17 (17 female) rhesus monkeys (Macaca mulatta) with a total of 17 scans. Structural MRIs were collected every 3 months from 2.63 years (31.56 months) of age to 30.64 years of age. All surgical and animal use procedures were reviewed and approved by the Institutional Animal Care and Use Committees of Wake Forest University, in accordance with the U.S. Public Health Service Policy on Humane Care and Use of Laboratory Animals and the National Research Council's Guide for the Care and Use of Laboratory Animals.

In preparation for the MRI scan, anesthesia was induced using ketamine (5–10 mg/kg) and dexmedetomidine (0.015mg/kg), and was maintained using isoflurane. The animals were

intubated and artificially ventilated at about 20 breaths per minute. Expired CO2 was monitored and maintained between 35 and 45 mmHg. Animals were scanned under isoflurane anesthesia at 1%–1.5%. Heart rate and oxygen saturation levels were monitored using a pulse oximeter. Their body temperature was maintained using warm blankets. The MRI system was a 3 Tesla Siemens MAGNETOM Skyra (Siemens Healthcare, Erlangen, Germany). Anatomical images were acquired using a T1-weighted MPRAGE sequence: TR = 2700 ms, TE = 3.32 ms, inversion time = 880, FOV = 128 × 128 mm, 192 slices of 0.5 mm thickness, resolution = 0.5 mm isotropic.

7. Affiliations of authors

[1]Center for the Integrative Developmental Neuroscience, Child Mind Institute. [2]Child Mind Institute. [3]University of Minnesota. [4]University of Cambridge, Department of Psychology. [5]University of Pennsylvania. [6]Nathan Kline Institute. [7]Queens University. [8]Department of Child and Adolescent Psychiatry and Behavioral Science, Children's Hospital of Philadelphia. [9]Department of Psychiatry, University of Pennsylvania. [10]Department of Psychiatry and Behavioral Sciences and The MIND Institute. [11]University of California Davis. [12]Stem Cell and Brain Research Institute. [13]Newcastle University. [14]Section on Comparative Medicine, Wake Forest University School of Medicine. [15]Universite Claude Bernard Lyon 1. [16]University of California Davis, Dept of Psychology. [17]Translational Neuroscience division, Center for Biomedical Imaging and Neuromodulation, Nathan Kline Institute. [18]University Medical Center Utrecht. [19]Columbia University. [20]Aix-Marseille University. [21]Translational Neuroscience Division, Center for Biomedical Imaging and Neuromodulation, Nathan Kline Institute. [22]Universite Claude Bernard Lyon1. [23]East China Normal University. [24]McGill University. [25]Department of Biomedical Engineering, Vanderbilt University. [26]NeuroSpin. [27]University of Illinois Urbana-Champaign. [28]University of Western Ontario. [29]Mount Sinai School of Medicine. [30]Rockefeller University. [31]Institute for Cognitive Science Marc Jeannerod. [32]University of Bristol. [33]University of Rochester. [34]Queen's University. [35]Institut des Sciences Cognitives Marc Jeannerod (ISC-MJ). [36]Lyon Neuroscience Research Center, University of Geneva. [37]Lyon Neuroscience Research Center, ImpAct Team. [38]Institut Pasteur. [39]Emory National Primate Research Center, Emory University. [40]Fralin Biomedical Research Institute, Virginia Tech. [41]Carilion Department of Human Development and Family Science, Virginia Tech. [42]University of Wisconsin Madison. [43]Oregon National Primate Research Center. [44]Princeton Neuroscience Institute & Department of Psychology, Princeton University. [45]Netherlands Institute for Neuroscience. [46]Emory National Primate Research Center; Emory University. [47]Abbott Laboratories. [48]Duke Kunshan University. [49]Centre for Social Learning and Cognitive Evolution, School of Biology, University of St. Andrews. [50]National Institute of Mental Health. [51]University of North Carolina at Chapel Hill. [52]Institute for Futures Studies, Stockholm, Sweden. [53]Centre for Cultural Evolution & Department of Zoology, Stockholm University, Sweden. [54]University of Oxford. [55]The University of Western Ontario. [56]California National Primate Research Center, Davis. [57]Department of Neuroscience, Icahn School of Medicine at Mount Sinai. [58]Oregon Health & Science University. [59]University of York. [60]Functional Imaging Laboratory, German Primate Center – Leibniz Institute for Primate Research. [61]Princeton Neuroscience Institute, Princeton University. [62]McGovern Institute for Brain Research, Massachusetts Institute of Technology. [63]Department of Biology, Utrecht University. [64]Department of Biology, McGill University. [65]INSERM Stem Cell & Brain Research Institute. [66]Department of Psychiatry & Behavioral Sciences, School of Medicine. [67]University of Fribourg, Switzerland. [68]Ruhr University Bochum, Faculty of Biology and Biotechnology, Cognitive Neurobiology. [69]Neural Circuits and Cognition Lab, European Neuroscience Institute Göttingen. [70]Perception and Plasticity Group, German Primate Center – Leibniz Institute for Primate Research. [71]Department of Bioengineering, Santa Clara University. [72]Department of Biology and Helmholtz Institute, Utrecht University. [73]Department of Computation and Neural Systems, California Institute of Technology. [74]Institute of Neuroscience. [75]State Key Laboratory of Primate Biomedical Research, Institute of Primate Translational Medicine, Kunming University of Science and Technology, Kunming, China. [76]Stem Cell & Brain Research Institute. [77]The Rockefeller University. [78]Krieger Mind/Brain Institute, Department of

Neurosurgery, Johns Hopkins University. [79]Newcastle University, University of Iowa. [80]French National Centre for Scientific Research. [81]Translational Neuroscience division, Center for Biomedical Imaging and Neuromodulation, Nathan Kline Institute. [82]Deptartment of Psychiatry, Neurology and Neurosurgery, Columbia University

8. Acknowledgements

T.X. was supported by the National Institutes of Health (NIH) RF1MH128696 and P50MH109429. M.P.M was supported by NIH R01MH111439, P50MH109429, MH124045, MH230482, and MH109429. R.A.I.B. was supported by the Academy of Medical Sciences, HDR UK. J.S. was supported by NIH R01MH134896, R01MH132934, and R01MH133843. A.F.A.-B. was supported by NIH R01MH134896, R01MH132934, and R01MH133843. A.R.F was supported by NCTRI P50MH109429. A.R.W was supported by NIDDK K01AG078407. A.F. was supported by NIH R01MH121735 and P51OD011107. A.T. was supported by New Frontiers in Research Fund (NFRFE) NFRFE-2021-00936. A.F. was supported by NIH R01MH111439 and P50MH109429. B.J. was supported by NIH R01MH134896, R01MH132934, and R01MH133843. B.B. was supported by NIH P50MH109429 and R01MH111439. B.E.R. was supported by NIH R01MH111439 and P50MH109429. B.R.H. was supported by NIH F31MH086203. C.M.D. was supported by NIH R01MH121735. C.M.S. was supported by the German Research Foundation (DFG) Emmy Noether program SCHW1683/2-1. C.R.E.W. was supported by Agende Nationale de la Recherche (ANR) ANR-18-CE37-0016-01 and ANR-11-LABX-0042. C.K. was supported by NIH P51OD011092. C.C. was supported by NIH R01MH116676 and R01MH117796. C.P. was supported by NC3Rs NC/K000802/1. D.A.L. was supported by NIMH ZICMH002899. D.G.A. was supported by NIH P51OD011107, R01MH041479, R01NS16980, R37MH57502, and California National Primate Research Center (CNPRC) grant RR000169. D.J.C. was supported by NFRFE-2021-00936. E.P. was supported by ANR-11-LABX-0042 and ANR-10-SVSE4-1141. E.C.S.E. was supported by ANR-15-CE17-0020, ANR-21-CE17-0028, ANR-16-RHUS-0009, and ANR-11-EQPX-0026. G.L. was supported by NIH RF1MH123202. G.L. was supported by NIH R01MH111439. G.B. was supported by ANR-11-LABX-0063. J.G. was supported by NFRFE-2021-00936. J.S. was supported by ANR-21-CE37-0016, and the Sir Henry Dale Wellcome Trust Fellowship 105651/Z/14/Z. J.K. was supported by NIH NIH T32AA007468. K.K.S. was supported by NIH T32GM007356. K.M. was supported by NIH P50MH109429 and R01MH111439. L.D. was supported by NIH R01MH134896, R01MH132934, and R01MH133843. L.J.C. was supported by NIH R01MH121735. M.M.S. was supported by NIH P50MH078105, R21HD055255, and P51OD011132. M.G.B. was supported by NIH P01AG016765. M.N. was supported by NIH P51OD011092. M.S. was supported by NIH R01MH091645, and P50HD103573. M.C.S. was supported by the Swiss National Science Foundation (SNSF) BSET-0_201532, 310030_204544, and the European Research Council (ERC) 637638 OptoVision. O.B. was supported by NIH P50MH109429 and R01MH111439. R.S.M. was supported by the Canadian Institute of Health Research (CIHR) FDN-148453. R.H. was supported by P50MH109429. R.V. was supported by NIH R01MH091645 and P50HD103573. S.K. was supported by NIH P50MH132642, R01MH137624, and R01 EY017699. S.F-W. was supported by the Biotechnology and Biological Sciences Research Council (BBSRC) BB/X013243/1 and a Bristol Neuroscience of Mental Health Award. S.B.H. was supported by ANR-16-CE37-0009-01, ANR-11-LABX-0042, and ANR-11-IDEX-0007. S.C.K. was supported by Jiangsu Provincial Department of Science and Technology BK20221267. C.I.P. was supported by the National Science Foundation (NSF) 2342847, and the Medical Research Council MR-T032553-1. C.S. was supported by NIH R01MH111439 and P50MH109429. Data were curated and analyzed using the Pittsburgh Supercomputing Center (BIO220056) through the Advanced Cyberinfrastructure Coordination Ecosystem: Services and Support (https://access-ci.org). We acknowledge the contribution from open datasets used in this study: the PRIMatE Data Exchange (PRIME-DE)

(https://fcon_1000.projects.nitrc.org/indi/indiPRIME.html) and the UNC-Wisconsin Neurodevelopment Rhesus Macaque MRI Database (https://www.nitrc.org/projects/uncuw_macdevmri). We thank Dr. Leslie Ungerleider and Paula L. Croxson for their contributions by providing the NHP data. We also express our deep appreciation to all the facility staff who assisted with the NHP data collection and acquisition.

9. References

1. Liu, Z. *et al.* Anatomical and diffusion MRI brain atlases of the fetal rhesus macaque brain at 85, 110 and 135 days gestation. *Neuroimage* **206**, 116310 (2020).
2. Bethlehem, R. A. I. *et al.* Brain charts for the human lifespan. *Nature* **604**, 525–533 (2022).
3. Markov, N. T. *et al.* A weighted and directed interareal connectivity matrix for macaque cerebral cortex. *Cereb. Cortex* **24**, 17–36 (2014).
4. Tustison, N. J. *et al.* The ANTsX ecosystem for quantitative biological and medical imaging. *Sci. Rep.* **11**, 9068 (2021).
5. Wang, X. *et al.* U-net model for brain extraction: Trained on humans for transfer to non-human primates. *Neuroimage* **235**, 118001 (2021).
6. Autio, J. A. *et al.* Towards HCP-Style macaque connectomes: 24-Channel 3T multi-array coil, MRI sequences and preprocessing. *Neuroimage* **215**, 116800 (2020).
7. Donahue, C. J. *et al.* Using Diffusion Tractography to Predict Cortical Connection Strength and Distance: A Quantitative Comparison with Tracers in the Monkey. *J. Neurosci.* **36**, 6758–6770 (2016).
8. Glasser, M. F. *et al.* The minimal preprocessing pipelines for the Human Connectome Project. *Neuroimage* **80**, 105–124 (2013).
9. Wang, H. *et al.* Multi-Atlas Segmentation with Joint Label Fusion. *IEEE Trans. Pattern Anal. Mach. Intell.* **35**, 611–623 (2013).
10. Fischl, B. FreeSurfer. *Neuroimage* **62**, 774–781 (2012).
11. Zhang, Y., Parmigiani, G. & Johnson, W. E. ComBat-seq: batch effect adjustment for RNA-seq count data. *NAR Genom Bioinform* **2**, lqaa078 (2020).
12. Xia, J., Wang, F., Wang, Y., Wang, L. & Li, G. Longitudinal mapping of the development of cortical thickness and surface area in rhesus macaques during the first three years. *Proc. Natl. Acad. Sci. U. S. A.* **120**, e2303313120 (2023).
13. Mikis Stasinopoulos, D. & Rigby, R. A. Generalized Additive Models for Location Scale and Shape (GAMLSS) in R. *J. Stat. Softw.* **23**, 1–46 (2008).
14. Djennad, A., Rigby, R., Stasinopoulos, M. & Voudouris, V. Detrended Transformed Owen's Plot: a diagnostic tool for checking the adequacy of a fitted model distribution. Preprint at https://www.researchgate.net/profile/Abdelmajid-Djennad/publication/277555041_Detrended_Transformed_Owen%27s_Plot_a_diagnostic_tool_for_checking_the_adequacy_of_a_fitted_model_distribution/links/556c69c608aec2268304eaeb/Detrended-Transformed-Owens-Plot-a-diagnostic-tool-for-checking-the-adequacy-of-a-fitted-model-distribution.pdf.
15. Yarkoni, T., Poldrack, R. A., Nichols, T. E., Van Essen, D. C. & Wager, T. D. Large-scale automated synthesis of human functional neuroimaging data. *Nat. Methods* **8**, 665–670 (2011).
16. Margulies, D. S. *et al.* Situating the default-mode network along a principal gradient of macroscale cortical organization. *Proc. Natl. Acad. Sci. U. S. A.* **113**, 12574–12579 (2016).
17. Bodin, C. *et al.* Functionally homologous representation of vocalizations in the auditory cortex of humans and macaques. *Curr. Biol.* **31**, 4839–4844.e4 (2021).
18. Wang, L. *et al.* Mixed selectivity coding of content-temporal detail by dorsomedial posterior parietal neurons. *J. Neurosci.* **44**, JN–RM–1677–23 (2024).
19. Cai, Y. *et al.* Time-sensitive prefrontal involvement in associating confidence with task performance illustrates metacognitive introspection in monkeys. *Commun. Biol.* **5**, 799 (2022).
20. Shi, Y. *et al.* UNC-Emory infant atlases for macaque brain image analysis: Postnatal brain development through 12 months. *Front. Neurosci.* **10**, 617 (2016).
21. Mavigner, M. *et al.* Postnatal Zika virus infection is associated with persistent abnormalities in brain structure, function, and behavior in infant macaques. *Sci. Transl. Med.* **10**, (2018).

22. Howell, B. R. *et al.* Disentangling the effects of early caregiving experience and heritable factors on brain white matter development in rhesus monkeys. *NeuroImage* **197**, 625–642 (2019).
23. Morin, E. L. *et al.* Developmental outcomes of early adverse care on amygdala functional connectivity in nonhuman primates. *Dev. Psychopathol.* **32**, 1579–1596 (2020).
24. Kovacs-Balint, Z. A. *et al.* Structural development of cortical lobes during the first 6 months of life in infant macaques. *Dev. Cogn. Neurosci.* **48**, 100906 (2021).
25. McCormack, K. M. *et al.* The developmental consequences of early adverse care on infant macaques: A cross-fostering study. *Psychoneuroendocrinology* **146**, 105947 (2022).
26. Lv, Q. *et al.* Large-scale persistent network reconfiguration induced by ketamine in anesthetized monkeys: Relevance to mood disorders. *Biol. Psychiatry* **79**, 765–775 (2016).
27. Froudist-Walsh, S. *et al.* The rhesus monkey hippocampus critically contributes to scene memory retrieval, but not new learning. *J. Neurosci.* **38**, 7800–7808 (2018).
28. Young, J. T. *et al.* The UNC-Wisconsin Rhesus Macaque Neurodevelopment Database: A Structural MRI and DTI Database of Early Postnatal Development. *Front. Neurosci.* **11**, 29 (2017).
29. Ortiz-Rios, M., Balezeau, F., Haag, M., Schmid, M. C. & Kaiser, M. Dynamic reconfiguration of macaque brain networks during natural vision. *Neuroimage* **244**, 118615 (2021).
30. Rinne, T., Muers, R. S., Salo, E., Slater, H. & Petkov, C. I. Functional imaging of audio-visual selective attention in monkeys and humans: How do lapses in monkey performance affect cross-species correspondences? *Cereb. Cortex* **27**, 3471–3484 (2017).
31. Poirier, C. *et al.* Auditory motion-specific mechanisms in the primate brain. *PLoS Biol.* **15**, e2001379 (2017).
32. Slater, H. *et al.* Individually customisable non-invasive head immobilisation system for non-human primates with an option for voluntary engagement. *J. Neurosci. Methods* **269**, 46–60 (2016).
33. Wilson, B. *et al.* Auditory sequence processing reveals evolutionarily conserved regions of frontal cortex in macaques and humans. *Nat. Commun.* **6**, 8901 (2015).
34. Baumann, S. *et al.* The topography of frequency and time representation in primate auditory cortices. *Elife* **4**, e03256 (2015).
35. Schönwiesner, M., Dechent, P., Voit, D., Petkov, C. I. & Krumbholz, K. Parcellation of human and monkey core auditory cortex with fMRI pattern classification and objective detection of tonotopic gradient reversals. *Cereb. Cortex* **25**, 3278–3289 (2015).
36. Russ, B. E. & Leopold, D. A. Functional MRI mapping of dynamic visual features during natural viewing in the macaque. *Neuroimage* **109**, 84–94 (2015).
37. Russ, B. E., Kaneko, T., Saleem, K. S., Berman, R. A. & Leopold, D. A. Distinct fMRI responses to self-induced versus stimulus motion during free viewing in the macaque. *J. Neurosci.* **36**, 9580–9589 (2016).
38. Park, S. H. *et al.* Functional subpopulations of neurons in a macaque face patch revealed by single-unit fMRI mapping. *Neuron* **95**, 971–981.e5 (2017).
39. Seidlitz, J. *et al.* A population MRI brain template and analysis tools for the macaque. *Neuroimage* **170**, 121–131 (2018).
40. Xu, T. *et al.* Delineating the macroscale areal organization of the macaque cortex in vivo. *Cell Rep.* **23**, 429–441 (2018).
41. Neudecker, V. *et al.* Early-in-life isoflurane exposure alters resting-state functional connectivity in juvenile non-human primates. *Br. J. Anaesth.* **131**, 1030–1042 (2023).
42. Liu, Z. *et al.* The effects of breastfeeding versus formula-feeding on cerebral cortex maturation in infant rhesus macaques. *Neuroimage* **184**, 372–385 (2019).
43. Noonan, M. P. *et al.* A neural circuit covarying with social hierarchy in macaques. *PLoS Biol.* **12**, e1001940 (2014).

44. Sallet, J. *et al.* Social network size affects neural circuits in macaques. *Science* **334**, 697–700 (2011).
45. Sallet, J. *et al.* Behavioral flexibility is associated with changes in structure and function distributed across a frontal cortical network in macaques. *PLoS Biol.* **18**, e3000605 (2020).
46. Schwiedrzik, C. M., Zarco, W., Everling, S. & Freiwald, W. A. Face patch resting state networks link face processing to social cognition. *PLoS Biol.* **13**, e1002245 (2015).
47. Wilson, C. R. E. *et al.* Prefrontal markers and cognitive performance are dissociated during progressive dopamine lesion. *PLoS Biol.* **14**, e1002576 (2016).
48. Stoll, F. M., Fontanier, V. & Procyk, E. Specific frontal neural dynamics contribute to decisions to check. *Nat. Commun.* **7**, 11990 (2016).
49. Faraut, M. C. M., Procyk, E. & Wilson, C. R. E. Learning to learn about uncertain feedback. *Learn. Mem.* **23**, 90–98 (2016).
50. Stoll, F. M. *et al.* The effects of cognitive control and time on frontal beta oscillations. *Cereb. Cortex* **26**, 1715–1732 (2016).
51. Vezoli, J. *et al.* Increased DAT binding in the early stage of the dopaminergic lesion: a longitudinal [11C]PE2I binding study in the MPTP-monkey. *Neuroimage* **102 Pt 2**, 249–261 (2014).
52. Fifel, K. *et al.* Alteration of daily and circadian rhythms following dopamine depletion in MPTP treated non-human primates. *PLoS One* **9**, e86240 (2014).
53. Khamassi, M., Enel, P., Dominey, P. F. & Procyk, E. Medial prefrontal cortex and the adaptive regulation of reinforcement learning parameters. *Prog. Brain Res.* **202**, 441–464 (2013).
54. Vezoli, J. *et al.* Early presymptomatic and long-term changes of rest activity cycles and cognitive behavior in a MPTP-monkey model of Parkinson's disease. *PLoS One* **6**, e23952 (2011).
55. Vezoli, J. & Procyk, E. Frontal feedback-related potentials in nonhuman primates: modulation during learning and under haloperidol. *J. Neurosci.* **29**, 15675–15683 (2009).
56. Grayson, D. S., Bliss-Moreau, E., Bennett, J., Lavenex, P. & Amaral, D. G. Neural reorganization due to neonatal amygdala lesions in the rhesus monkey: Changes in morphology and network structure. *Cereb. Cortex* **27**, 3240–3253 (2017).
57. Hunsaker, M. R. & Amaral, D. G. A semi-automated pipeline for the segmentation of rhesus macaque hippocampus: validation across a wide age range. *PLoS One* **9**, e89456 (2014).
58. Hunsaker, M. R., Scott, J. A., Bauman, M. D., Schumann, C. M. & Amaral, D. G. Postnatal development of the hippocampus in the Rhesus macaque (Macaca mulatta): a longitudinal magnetic resonance imaging study. *Hippocampus* **24**, 794–807 (2014).
59. Schumann, C. M., Scott, J. A., Lee, A., Bauman, M. D. & Amaral, D. G. Amygdala growth from youth to adulthood in the macaque monkey. *J. Comp. Neurol.* **527**, 3034–3045 (2019).
60. Scott, J. A. *et al.* Longitudinal analysis of the developing rhesus monkey brain using magnetic resonance imaging: birth to adulthood. *Brain Struct. Funct.* **221**, 2847–2871 (2016).
61. Holley, D. *et al.* Rhesus infant nervous temperament predicts peri-adolescent central amygdala metabolism & behavioral inhibition measured by a machine-learning approach. *Transl. Psychiatry* **14**, 148 (2024).
62. Tromp, D. P. M., Fox, A. S., Oler, J. A., Alexander, A. L. & Kalin, N. H. The Relationship Between the Uncinate Fasciculus and Anxious Temperament is Evolutionarily Conserved and Sexually Dimorphic. *Biological psychiatry* **86**, 890 (2019).
63. Fox, A. S. *et al.* Functional connectivity within the primate extended amygdala is heritable and associated with early-life anxious temperament. *J. Neurosci.* **38**, 7611–7621 (2018).
64. Fox, A. S. *et al.* Intergenerational neural mediators of early-life anxious temperament. *Proc. Natl. Acad. Sci. U. S. A.* **112**, 9118–9122 (2015).

65. Birn, R. M. *et al.* Evolutionarily conserved prefrontal-amygdalar dysfunction in early-life anxiety. *Mol. Psychiatry* **19**, 915–922 (2014).
66. Shackman, A. J. *et al.* Neural mechanisms underlying heterogeneity in the presentation of anxious temperament. *Proc. Natl. Acad. Sci. U. S. A.* **110**, 6145–6150 (2013).
67. Rogers, J. *et al.* CRHR1 genotypes, neural circuits and the diathesis for anxiety and depression. *Mol. Psychiatry* **18**, 700–707 (2013).
68. Fox, A. S. *et al.* Central amygdala nucleus (Ce) gene expression linked to increased trait-like Ce metabolism and anxious temperament in young primates. *Proc. Natl. Acad. Sci. U. S. A.* **109**, 18108–18113 (2012).
69. Oler, J. A. *et al.* Amygdalar and hippocampal substrates of anxious temperament differ in their heritability. *Nature* **466**, 864–868 (2010).
70. Roseboom, P. H. *et al.* Neuropeptide Y receptor gene expression in the primate amygdala predicts anxious temperament and brain metabolism. *Biol. Psychiatry* **76**, 850–857 (2014).
71. Grier, M. D. *et al.* Ultra-high field (10.5T) diffusion-weighted MRI of the macaque brain. *Neuroimage* **255**, 119200 (2022).
72. Lagore, R. L. *et al.* An 8-dipole transceive and 24-loop receive array for non-human primate head imaging at 10.5 T. *NMR Biomed.* **34**, e4472 (2021).
73. Yacoub, E. *et al.* Ultra-high field (10.5 T) resting state fMRI in the macaque. *Neuroimage* **223**, 117349 (2020).
74. Zitella, L. M. *et al.* Subject-specific computational modeling of DBS in the PPTg area. *Front. Comput. Neurosci.* **9**, 93 (2015).
75. Zitella, L. M. *et al.* In vivo 7T MRI of the non-human primate brainstem. *PLoS One* **10**, e0127049 (2015).
76. Hutchison, R. M., Hashemi, N., Gati, J. S., Menon, R. S. & Everling, S. Electrophysiological signatures of spontaneous BOLD fluctuations in macaque prefrontal cortex. *Neuroimage* **113**, 257–267 (2015).
77. Zhu, J. *et al.* Brain structure and activity predicting cognitive maturation in adolescence. *bioRxivorg* 2024.08.23.608315 (2024).